Sedimentary Geology 353 (2017) 139–157

Contents lists available at ScienceDirect

Sedimentary Geology

journal homepage: www.elsevier.com/locate/sedgeo

Paleo-climatic and paleo-environmental evolution of the Neoproterozoic basal sedimentary cover on the Río de La Plata Craton, Argentina: Insights from the $\delta^{13}C$ chemostratigraphy

Lucía E. Gómez-Peral [a,*], Alcides N. Sial [b], M. Julia Arrouy [a], Sebastián Richiano [a], Valderez P. Ferreira [b], Alan J. Kaufman [c], Daniel G. Poiré [a]

[a] Centro de Investigaciones Geológicas - CONICET-UNLP –, Argentina
[b] NEG-LABISE, Department of Geology, Federal University of Pernambuco, Recife, Brazil
[c] Department of Geology, ESSIC, University of Maryland, College Park, MD, USA

ARTICLE INFO

Article history:
Received 1 December 2016
Received in revised form 13 March 2017
Accepted 14 March 2017
Available online 18 March 2017

Editor: Dr. B. Jones

Keywords:
Carbon isotopes
Cryogenian stromatolitic dolostones
Redox
Cap carbonate
Tandilia

ABSTRACT

The Sierras Bayas Group of the Tandilia System constitutes the Neoproterozoic sedimentary cover of the Río de La Plata Craton in Argentina that accumulated amid the breakup of the Rodinia supercontinent and subsequent assembly of Gondwanaland. Evidence for glaciation in the Villa Mónica Formation (VMF) at the base of the succession comes in the form of iron-rich laminated sediments containing dropstones composed predominantly of basement crystalline rocks and quartzites that, are sequentially overlain by a phosphatic mudstone and a ~40 m thick stromatolitic dolomite. Subtidal facies preserve columnar forms similar to post-glacial tubestone stromatolites seen in the Neoproterozoic records. These morphologies suggest rapid growth associated with elevated seawater alkalinity and high rates of carbonate accumulation records. The VMF dolomites in our four studied sections near Olavarría-Sierras Bayas area reveal a pronounced negative-to-positive $\delta^{13}C$ up section that is similarly to these cap carbonates and others worldwide. Our sedimentological and geochemical study of the VMF sections reveal consistent carbon and oxygen isotope trends that may be useful for detailed intra-basinal correlations. Samples of the VMF fabric-retentive dolomite preserve an unusually narrow range of non-radiogenic strontium isotopic compositions (0.7068 to 0.7070) that are consistent with Cryogenian limestone facies in the potential Namibian and Brazilian equivalents. Exceptional preservation of $^{87}Sr/^{86}Sr$ compositions suggest the possibility of primary dolomite precipitation in post-glacial seawater, and furthermore that REE patterns and distributions may yield similar insights to redox conditions in the depositional basin. In particular, the VMF dolomites reveal depleted LREE abundances, a negative Ce anomaly, positive La and Gd anomalies, and low Y/Ho values. As a whole, these observations suggest oxidizing post-glacial seawater conditions associated with significant freshwater inputs into the basin. Global warming and increases in primary productivity and organic carbon burial linked to the buildup of oxygen, the positive $\delta^{13}C$ trend and the increase in stromatolite biodiversity in the VMF.

1. Introduction

Neoproterozoic strata contain evidence for the breakup of the Rodinia supercontinent, widespread glaciation, high-amplitude fluctuations in geochemical proxy records, and the radiation of eukaryotic algae to ecological prominence (Knoll et al., 2006). However, age uncertainties have precluded a better understanding of the nature and interrelationships of these events (Macdonald et al., 2010).

Where radiometric constraints are available, the Cryogenian Period appears to include the interval between ~720 and 635 Ma (Rooney et al., 2005).

As these successions are normally unfossiliferous and poorly dated, carbon and strontium isotope data have become powerful tools for correlation within a sedimentary basin or even at global scale (Hoffman and Schrag, 2002). The term 'cap dolostone' is commonly used to describe dolomitic units associated with glacigenic deposits in Neoproterozoic successions. Systematic sedimentological and geochemical analysis of carbonate rocks (mostly dolomite) shows that it is possible to characterize such units by their specific mineralogical, sedimentological, petrographic, geochemical and stratigraphic features (Corkeron, 2007).

* Corresponding author at: Centro de Investigaciones Geológicas, Universidad Nacional de La Plata, diagonal 113 # 275, 1900 La Plata, Argentina.
E-mail address: lperal@cig.museo.unlp.edu.ar (L.E. Gómez-Peral).

http://dx.doi.org/10.1016/j.sedgeo.2017.03.007
0037-0738/

Carbon isotope ratios of Neoproterozoic successions worldwide placed just at the end of a glacial event show $\delta^{13}C$ excursions from negative to positive values (e.g., Kaufman et al., 1997; Kennedy et al., 1998; Hoffman et al., 1998). Across the same intervals, Sr-isotope data are interpreted to reflect $^{87}Sr/^{86}Sr$ variation of contemporary seawater during deposition of different carbonate sequences in the Neoproterozoic. The lowest $^{87}Sr/^{86}Sr$ values (0.7056) are consistent with 850–750 Ma seawater and higher values (0.7074 to 0.7087) with latest Neoproterozoic seawater (e.g., Jacobsen and Kaufman, 1999; Brasier and Shields, 2000; Melezhik et al., 2001; Thomas et al., 2004; Hoffman et al., 2007; Halverson et al., 2007). $^{87}Sr/^{86}Sr$ ratios are ≤0.7064 in East Greenland and ≤0.7068 in NE Svalbard, consistent with early Cryogenian values globally and inconsistent with late Cryogenian ratios, which are exclusively ≥0.7071 (Hoffman et al., 2012). In this period, dolomite predominates over limestone platforms with high stromatolite diversity and positive anomalies that are important for global correlation (Grey et al., 2011).

Apart from that, a stratigraphic pattern of C isotopic change reconstructed from numerous samples from different localities, and with different mineralogical, textural and geochemical characteristics has been assumed as a strong indicator of a robust signal (Kaufman and Knoll, 1995). Moreover, marine chemical sediments typically reflect the seawater trace and rare earth elements plus yttrium (REY) composition (e.g., Shields and Webb, 2004; Bolhar and Van Kranendonk, 2007; Frimmel, 2009) constituting another possible source of evidence of environmental changes.

On top of that, at the Río de La Plata Craton, the Villa Mónica Formation (VMF) is the only unit in Argentina that could testify all of these worldwide-identified Neoproterozoic events. The deposits of the VMF are divided into two informal sections; the lower siliciclastic section composed by conglomerates, sandstones, wackestones, diamictites and shales with phosphates, and the upper section mainly constituted by stromatolitic and laminated dolostones. In addition, the VMF is eroded at the top by a karstic surface which is a very important discordance that could even represent a ~200 Ma period of erosion (Gómez Peral et al., 2011).

New C– and O-isotope data from three different sections of the VMF are reportedrepor in this study, together with major, trace, and rare earth element concentrations dolostones. Previous $\delta^{13}C$ values from the dolostones (Gómez Peral et al., 2007) were interpreted as a product of diagenetic overprinting. However, in the light of the data from this study, we believe that this interpretation should be reevaluated.

The main goals of this contribution are: (a) generate a model of palaeoenvironmental evolution supported bydetailed sedimentological analysis, combined with geochemical data; (b) report new results of strong negative to positive $\delta^{13}C$ up section trend in tubestone-dolomites above a diamictite with dropstones, arrive to looking for most accurate interpretation; (c) examining oxygen level conditions and probable interaction with post depositional fluids; and (d) illustrate the chemostratigraphic correlation between different sections of the dolomitic deposits from the Tandilia Basin allows to indicate its relation to extreme climate oscillations and sea level fluctuations characteristic of the Cryogenian Period.

2. Geological setting

The VMF is part of the Tandilia System is a 350 km long, northwest to southeast oriented, orographic belt, located in the Buenos Aires province (Fig. 1). The System comprises an igneous-metamorphic basement covered by Neoproterozoic to Lower Palaeozoic sedimentary rocks. The basement rocks are composed of granitoids, orthogneisses and migmatites of the Buenos Aires Complex, which has a range of Sm—Nd model ages of 2440–2668 Ma (Transamazonian) by U—Pb SHRIMP (Cingolani et al., 2002) and Sm—Nd model ages averaging 2.6 Ga (Pankhurst et al., 2003).

In the Olavarría area, the Neoproterozoic sedimentary cover is ~435 m thick (Poiré, 1987, 1993; Iñiguez Rodríguez, 1999; Poiré and Spalletti, 2005; Gómez Peral et al., 2007, 2011; Arrouy et al., 2015; Fig. 1b) and is represented by the Sierras Bayas Group (Villa Mónica, Colombo, Cerro Largo, Olavarría and Loma Negra formations ~185 m; Fig. 1) and the La Providencia Group (Avellaneda, Alicia and Cerro Negro Formations, ~250 m; Arrouy et al., 2015, Fig. 2). The oldest depositional unit, Villa Mónica Formation (Figs. 2, 3a-k) is divided in two sections: (a) lower VMF composed mainly by siliciclastic conglomerates and sandstones-wackestones at the base and the upper VMF(b) dolostones including shallow-marine stromatolites and shale-marls at the top (Figs. 2, 3). Acritarchs assemblage occurring in greenish claystones of the upper VMF was assigned to *Leiosphaeridia minuttisima, L. tenuissima* and *Synsphaeridium sp.* (up to 450 μm in diameter; Gaucher et al., 2005).

The depostion of Villa Mónica Formation predates the amalgamation of Gondwana (Rapela et al., 2011) and likely accumulated in response to rifting associated with the breackup of Rodinia (Johansson, 2014).

The geochronological data available for the Sierras Bayas Group are sparse and somewhat controversial. The VMF host an important stromatolite assemblage constituted by *Colonella fm., Conophyton?resotti, Conophyton fm., Cryptozoon fm., Gongylina fm., Gymnosolem fm., Inzeria fm., Jacutophyton fm., Jurusonia nisvensis, Katavia fm., Kotuikania fm., Kussiella fm., Minjaria fm., Parmites fm., Parmites* cf. *cocrescens* and *Stratifera fm.* (Poiré, 1989, 1993), similar associations were described in numerous Tonian–Cryogenian successions (Cloud and Dardenne, 1973; Semikhatov, 1975, 1991; Knoll et al., 1991; Azmy et al., 2001; Batten et al., 2004; Halverson et al., 2007; Hoffman et al., 2012; Alvarenga et al., 2014; Grey et al., 2011). A minimum age for VMF of 793 ± 32 Ma (Rb—Sr) was suggested from interbedded fine-grained sedimentary rocks (Cingolani and Bonhomme, 1988) and interpreted as diagenetic overprint. Whole-rock Rb—Sr determinations on shale from this unit indicated an age of 725 ± 36 Ma (Kawashita et al., 1999). Similarly, Bonhomme and Cingolani (1980) reported an Rb—Sr age of 769 ± 12 Ma for the same unit. Detrital zircon ages for the Sierras Bayas Group were reported by Rapela et al. (2007), Gaucher et al. (2008) and Cingolani (2011), being the youngest detrital zircons of 1150 Ma (Rapela et al., 2007).

The recorded $^{87}Sr/^{86}Sr$ values from dolostones are between 0.7068 and 0.7070 (Gómez Peral et al., 2014), similar to other Cryogenian carbonates elsewhere in which they vary between 0.7060 and 0.7070 (Walter et al., 2000; Hill et al., 2000; Kaufman et al., 2009; Halverson et al., 2010).

The age of Loma Negra Formation is also debated, suggested firstly as ~540 Ma by Cloudina (Gaucher et al., 2005), however could be older considering $\delta^{13}C$ and $^{87}Sr/^{86}Sr$ combined trends ~580–590 Ma (Gómez Peral et al., 2007). Moreover, in the overlaying Cerro Negro Formation, top of La Providencia Group, Arrouy et al., 2016) have described typical morphs of *Aspidella* (related to the 560—550 Ma White Sea assemblage; Waggoner, 2003).

There are three important unconformities in the Sierras Bayas Group (Fig. 2) and middle one is of special significance for this study and has been called "Piedra Amarilla Surface" (Gómez Peral et al., 2011). It is located in the contact between the Villa Mónica and Colombo formations, allow separating the Sierras Bayas Group in two sections. According to Gómez Peral et al. (2011), different burial diagenetic histories in the siliciclastic units of the lower Sierras Bayas Group (VMF) with respect to the upper successions (Colombo, Cerro Largo and Olavarría formations; Fig. 2) can be recognized. The Piedra Amarilla surfaces also represents a long period of erosional and subaerial exposure, and is marked by a karstic surface (Gómez Peral et al., 2011), associated with breccias and diamictitic rocks. This important unconformity was set from paleomagnetic studies around 600 Ma (Rapalini et al., 2013) and interpreted as the age of important weathering event.

The upper discontinuity, "Barker surface", is on top of the Sierras Bayas Group and has been correlated to other Neoproterozoic surfaces

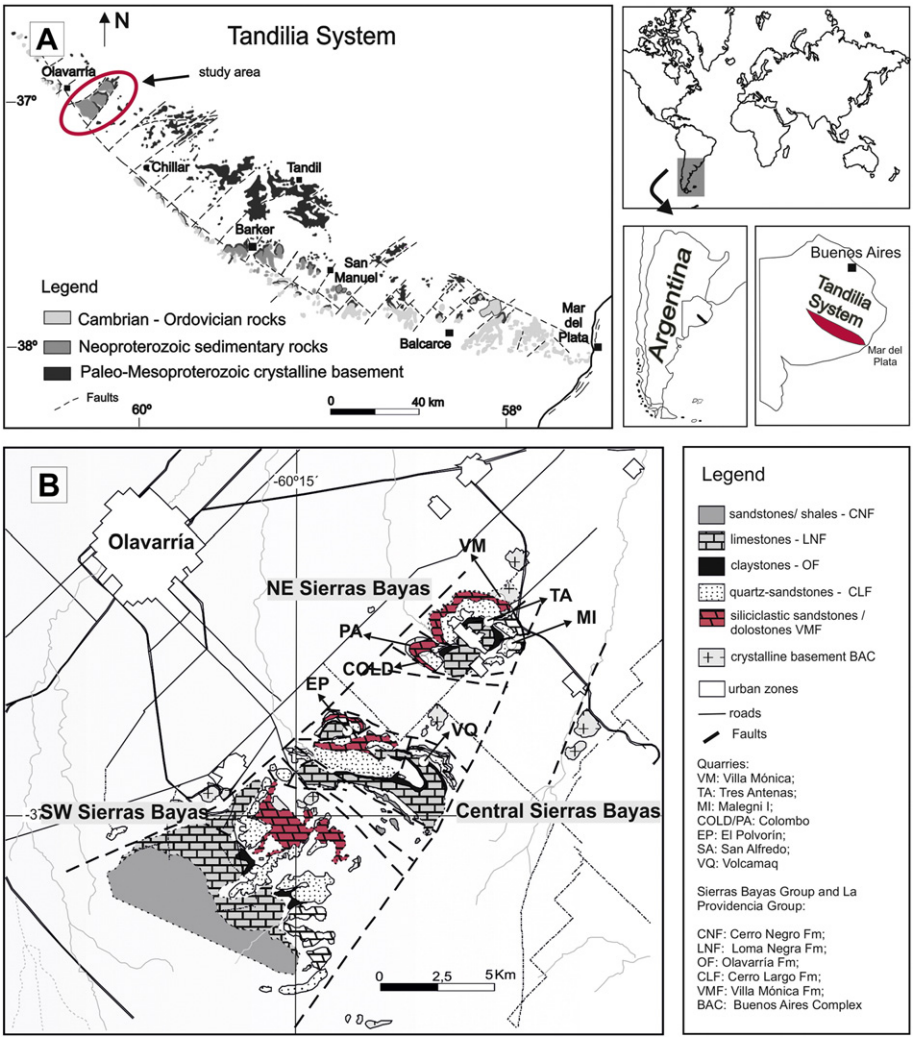

Fig. 1. (A): Study area in the Tandilia System, Buenos Aires Province, Argentina. (B) Geological map of the Sierras Bayas, Olavarría region, northwestern part of the Tandilia System (modified from Iñiguez Rodríguez, 1999; Gómez Peral et al., 2014).

in the SW of Gondwana in Uruguay, Brazil, South Africa and Namibia, and related tentatively to Gaskiers glaciation (Poiré et al., 2007).

2.1. Villa Mónica Formation

2.1.1. Villa Mónica sandstone-conglomerates

The basal section of the VMF (up to 22 m thick) is constituted by siliciclastic (quartz-arkosic) conglomerate-sandstones, observed in drill cores which cross cut the succession down to the contact with the basement (Poiré, 1987; Gómez Peral et al., 2011). The main detrital and authigenic components were exclusively sourced from the basement (Zimmermann et al., 2011). Gómez Peral et al. (2011) define their composition, textures and microstructures.

Below the dolostones, a pebbly iron-rich mudstone facies was recognized (Figs. 3A, B, D, 4 and 5) which is characterized by two marked textural modes (mudstone with floating pebbles: Fd) of less than a meter of thick, this was identified in one poor exposed section and in the subsoil (Fig. 3a-b). At the base of each pebble, mudstone is arched as if the clasts had dropped, also at microscopic scale (Gómez Peral et al., 2011, Fig. 6A). Textural bimodality as well as *syn*-sedimentary deformational microstructures suggest that the pebbles could be dropstones (Frakes and Francis, 1988; Bennett et al., 1996), associated to probable glaciomarine origin (Gómez Peral et al., 2011, 2014, Fig. 6A).

Above this diamictite, another facies was recognized characterized by black phosphate lenses and concretions with green and red shaly matrix (Ph), concentrated along bedding planes; these have previously been linked to phosphogenesis associated with Cryogenian glaciation (Figs. 3D, 4; Gómez Peral et al., 2014).

2.1.2. Villa Mónica Dolostones

The dolomitic succession (36–52 m thick; Fig. 4B, E–K) hosts a rich assemblage of stromatolites (Poiré, 1993). The variable thickness of the upper dolomitic succession can be mostly ascribed to the channeling between biostromes or bioconstructions on the top of the dolomitic-pelitic succession (Fig. 4B). In addition, Gómez Peral et al. (2011) have reported the presence of an important uplift related to a period of intense erosion and weathering with the generation of a karstic surface on top of the dolostones which constitutes a telodiagenetic surface (Fig. 3B).

The dolostones are represented by laminated and stromatolitic dolostones, interbedded with centimeter-scale green claystone beds and culminating with red marls with associated claystones (Fig. 3 C–K). The mineralogical composition of the Villa Mónica dolostones determined by X-ray diffraction (Gómez Peral, 2008) which indicates they are composed mostly by stoichiometricstoichiometric dolomite (75–95%), with scarce calcite (1–5%), quartz and chert (1–15%), clay minerals (2%) and feldspar (1%). Insoluble acid residue (IAR) ranges from 4.7% to 16.8% (Gómez Peral et al., 2007).

In addition, te VMF is eroded at the top by a karstic surface, which is a very important discordance that could even represent a ~200 Ma period of erosion (Gómez Peral et al., 2011; Rapalini et al., 2013).

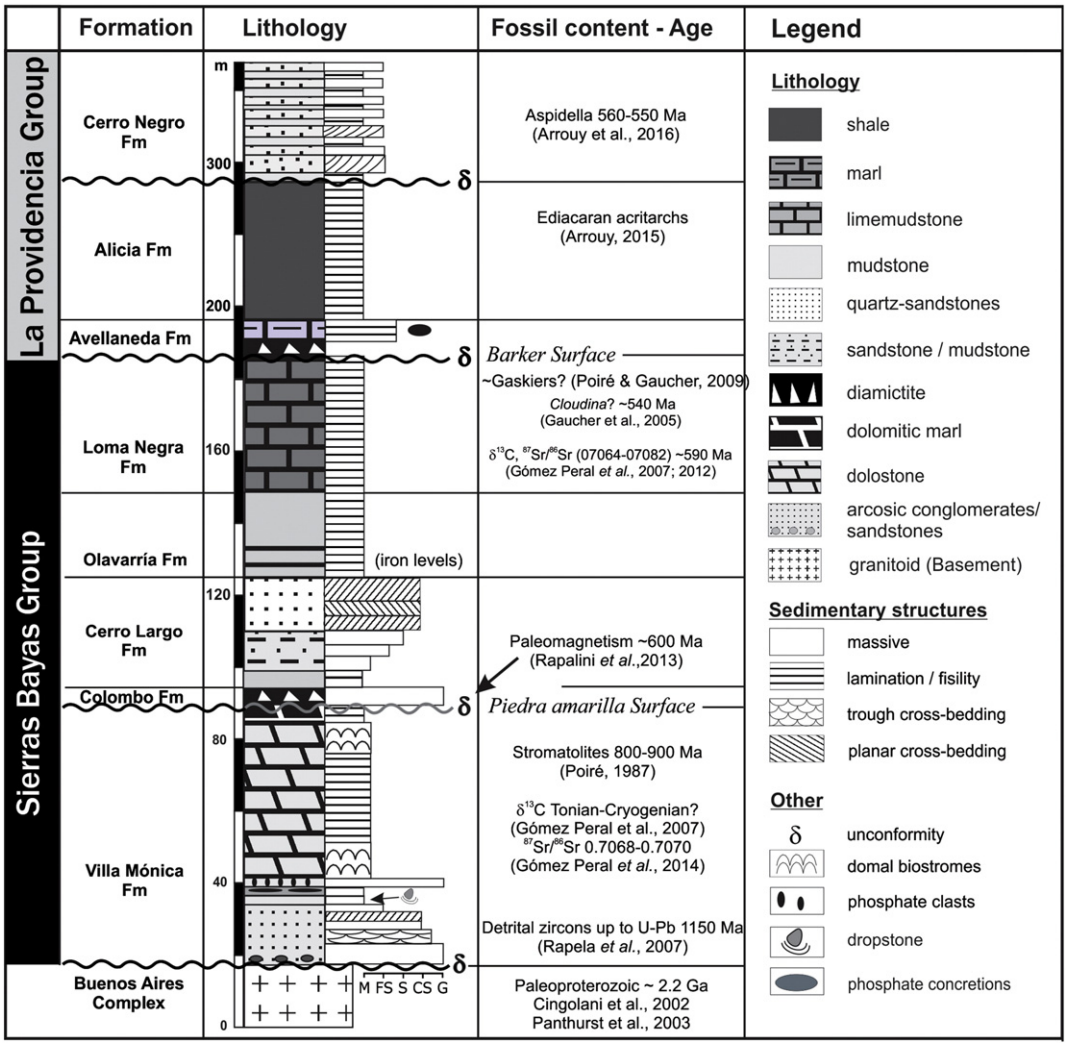

Fig. 2. Schematic representation of the Sierras Bayas and La Providencia groupsg (Gómez Peral et al., 2014 modified).

3. Sampling and analytical methods

The Villa Mónica dolostones have scarce outcrops as they are in closed relationship with subsurface ore activity, however, ten sections have been studied and sampled in quarries and subsurface cores. At the NE Sierras Bayas Hills three sections were studied from outcrops in quarries: one in Tres Antenas Quarry (D) and two in Piedra Amarilla/ Colombo Quarries (PA and COLD; Figs. 1B, 3B). On the other hand, in the Central Sierras Bayas Hills, near Olavarría locality, seven sections were sampled (one in the Volcamaq Quarry and six in the El Polvorín Quarry; Fig. 1B). The six sections from El Polvorín Quarry have been described from drill-cores (T1, T2, T3, T4, T5 and T6; Fig. 1B). Among all of these sections analyzed, the thicker one includes ~50 m of dolostones of the VMF (Fig. 3B), for that reason, it has been studied regarding sedimentary facies analyses, paleo-environmental characterization of the facies associations recorded, added to petrography and diagenesis.

Eighty-five polished thin sections were analyzed and stained with red S alizarin in order to differentiate between and within carbonates (Dickson, 1966).

Four of the studied sections were analyze for stable isotopes (COLD and PA in Colombo/Piedra Amarilla Quarry, and from the subsurface sections T3 and T6from El Polvorín Quarry) as they show the complete dolostone succession. Considering Colombo Quarry (COLD) the most complete section of the Upper VMF, 27 samples were analyzed by XRF (Table 1).

Forty-three samples of dolostones were analyzed for C and O isotopes (Tables 2, COLD; T3 and T6). These analyses were performed at the Stable Isotope Laboratory (LABISE) of the Department of Geology, Federal University of Pernambuco, Brazil. Extraction of CO_2 gas from powdered samples from selected unaltered microfacies (avoiding fractures, recrystallized portions and weathered surfaces: types IV to VI of dolomite; see below) was performed in a high-vacuum line after reaction with 100% orthophosphoric acid at 25 °C for one day (three days allowed, when dolomite was present). Released CO_2 was analyzed after cryogenic cleaning in double inlet, triple-collector SIRA II or Delta V Advantage mass spectrometers and results are reported in δ notation in permil (‰) relative to the VPDB standard. The uncertainties of the isotope measurements were better than 0.1‰ for carbon and 0.2‰ for

Fig. 3. Field photos from the Villa Mónica Formation and its sedimentary facies: (A) Fd = diamictite with droptones; (B) more detailed scale of Fd facies; (C) complete section of dolostones in the Colombo Quarry; (D) contact between lower and upper Villa Mónica Formation; pH = phosphates, Dbh = domal biohermal dolostones; (E) Gi = intraclast conglomerate with phosphate (black) and claystone (light green) pebbles; (F) Dbh with inner stratified stromatolites and interlayered claystones; (G) Dl = stratified/laminated dolostones; (H) Dbh associated with Dbe = domal biostrome and Cl = laminated claystones interbedded; (I) Sc: columnar stromatolites; (J) Do = microscope view of oolitic dolostone; (K) MCl: reddish and purple marls and claystone interbedded; (L) detail of a coarse-boulder clast in the Colombo Diamictite.

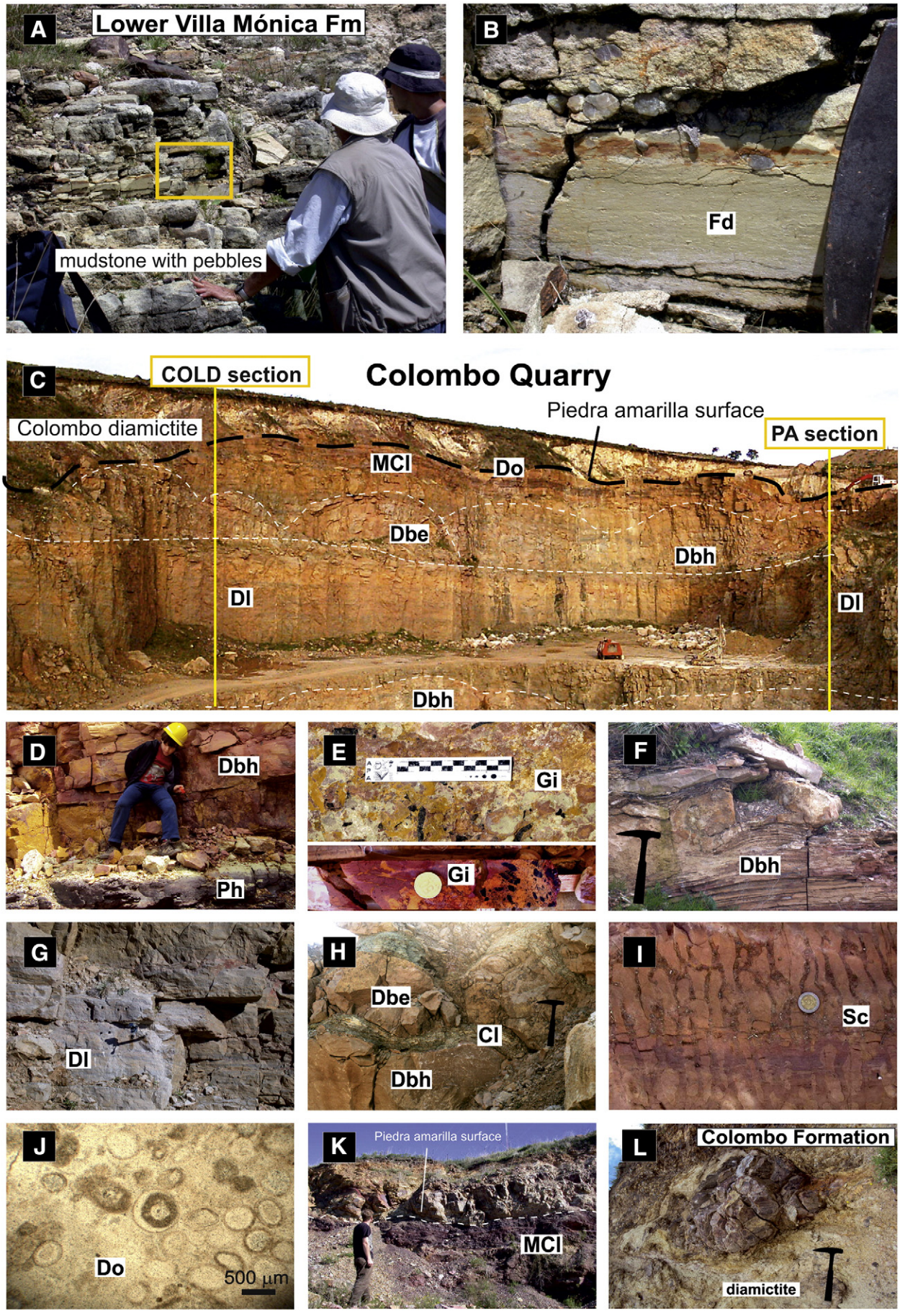
A
Lower Villa Mónica Fm
mudstone with pebbles
B
Fd
C
COLD section
Colombo Quarry
Piedra amarilla surface
Colombo diamictite
PA section
MCl
Do
Dbe
Dbh
Dl
Dl
Dbh
D
Dbh
Ph
E
Gi
Gi
F
Dbh
G
Dl
H
Dbe
Cl
Dbh
I
Sc
J
Do
500 μm
K
Piedra amarilla surface
MCl
L
Colombo Formation
diamictite

Lithofacies	Code	Description
Oolitic dolostone	Do	Ooolitic grainstone (~0.4 mts thick). Present yellow to brownish coloration. Ooids are from 0.5 to 1 mm in diameter, spherical to subspherical with irregular shapes and were completely silicified.
Marls and claystones	MCl	Red and purple interbeded marls and claystones (~2.5 mts thick), with planar lamination and medium bedding.
Domical dolomitic bioherms	Dbh	Formed by coalescence of subspheroidal, domal and columnar stromatolitic dolostones. Composed by dolomicrite and dolosparite of grey and yellow colorations. Domal stromatolite structures internally develops stratiform stromatolites.
Laminated dolostone	Dl	Planar lamination is related to banded dolomites show thin (~ 1 mm) interlayered dark and light layers, dark layer is a fine grained dolomicrite and clear bands show doloesparite.
Laminated claystone	Cl	Light green claystone up to 25 ctm of thick with planar lamination.
Domal dolomitic biostrome	Dbe	Domal biostrome, with inner bulbous and columnar stromatolites, are entirely constituted by yellow dolomicrite and dolosparite The internal structure are planar and wavy laminated.
Conglomerate	Gi	Intraclastic masive conglomerate in a dolomitic matrix. Poorly exposed (10-30 cm). Constituted by rounded to subrounded intraclasts of phosphates, claystones and quartzsandstones up to 3.5 cm in diameter.
Phosphate lenses	Ph	Black phosphate lenses (20-30 cm length) and concretions (5-8 cm diameter) with shaly matrix, (Gómez Peral et al., 2014).
Pebbly mundstone	Fd	Mudstone with discrete level of dropstones (floating pebbles) (Gómez Peral et al., 2011; 2014).

Facies Association	Facies	Depositional setting
3	Do-MCl	Lower intertidal to supratidal carbonate deposition with terrigenous supply under well oxigenated low to high energy conditions.
2	Gi-Dbe-Dbh-Cl-Dl	Subtidal carbonate (dolomite) deposition, alternating hight and low energy under oxic conditions.
1	Ph-Cl-Fd	Singlacial to deglacial siliciclastic sedimentation in outer shelf. Authigenic precipitation by upwelling currents. Suboxic stratified sea and low energy.

Fig. 4. Summary of facies and facies association description of the dolostones from the upper Villa Mónica Formation, added to some data from the lower Villa Mónica Formation (Gómez Peral et al., 2014).

oxygen, based on multiple analyses of an internal laboratory standard (BSC).

ICP-MS results of proxy trace elements (Mn, Sr and Rb) were analyzed and used to indicate the degree of preservation of C and O isotopes (Table 2).

Major element concentrations were analyzed by X-ray fluorescence spectrometry using fused beads and an automatic RIX-3000 (RIGAKU) unit available at the LABISE. Fused beads were prepared using Li fluoride and uncertainties were better than 5% for Fe and 10% for Mn. For all geochemical and isotope analyses in this study see Tables 1 and 2.

In preparation for elemental analyses, aliquots of powders were digested for 2 h in trace-metal grade 2% HNO_3. Solutions were centrifuged and decanted to remove insoluble residue. Precision and reproducibility for all elements analyzed are better than 10%, based on replicate measurements of laboratory calcite and dolomite standards.

Twenty-three (23) elemental analyses were performed in powdered dolostone samples (types I and II of dolomite; eight from the Colombo and fifteen from the Tres Antenas quarries).The samples were analyzed by ICP-MS using a Perkin-Elmer ICP-MS fitted with a Meinhardt concentric nebulizer of the Centro de Investigaciones Geológicas laboratories (CONICET-UNLP) to determine Mn, Sr, Rb (Table 2) and rare earth elements (REE) and yttrium expressed in ppm (Tables 2 and 3).

The Ce/Ce* ratios represent $3Ce_N/(2La_N + Nd_N)$ (Elderfield and Graves, 1982) while Ce anomaly is the log of Ce/Ce* (Bau and Dulski, 1996), and the Eu anomaly was calculated from Eu anom = $Eu_N/(0.67*Sm_N + 0.33*Tb_N)*0.5$ (Frimmel, 2009). $Y/Y^* = 2Y_N/(Dy_N + Ho_N)$, and $Pr/Pr^* = 2Pr_N/(Ce_N + NdN)$, where N refers to normalized concentrations relative to the standard post-Archean Australian Shale (McLennan, 1989), and $Gd/Gd^* = Gd/Gd = Gd/(2\,Tb - Dy)$ according to Frimmel (2009), (Table 3).

4. Analytical results

4.1. Villa Mónica dolostones

The occurrence of the Villa Mónica dolostones was registered in Piedra Amarilla ~ Colombo, Tres Antenas and Volcamaq quarries and drill cores from El Polvorín Quarry, where their thickness varies between 39 and 52 m (Figs. 1 and 5). Dolostones show mostly clear colorations with predominance of grey, yellow, and in less proportion dark coloration as brownish yellow and reddish. All dolomitic facies studied here are schematically represented and described in Fig. 4.

The basal dolomitic lithofacies is only recognized in one location at the floor of the Piedra Amarilla Quarry, where the underlying siliclastic section (green to red shales and phosphatic lenticular concretions) of the lower VMF is poorly exposed (Fig. 3D). The first few meters of the dolostones contain columnar stromatolites that grade upward along a diffuse and transitional contact to a grey laminated dolostone (Poiré, 1993; Gaucher and Poiré, 2009). This lower contact of the dolomites, rarely exposed, it was observed in drill cores up to the basement in the El Polvorín Quarry (Fig. 3D), that is difficult to pinpoint in the field, but generally identified by a switch from shales with phosphates and a thin intraclast conglomerate level (Fig. 3E).

A total of nine sedimentary facies have been recognized in the analyzed section (Figs. 3 and 5). In this facial scheme we include from base to top, the following:(1) Fd (mudstone with dropstones) and (2) Ph (phosphate lenses with shaly matrix)which mentioned before (Figs. 3A, B, D, 4 and 5), (3) intraclast conglomerates (Gi), (4) biostromal dolostones (Dbe), (5) laminated green claystonse (Cl), (6) laminated/stratified dolostones (Dl), (7) domical bioherm dolostones (Dbh), (8) purple laminated dolomitic marls interbedded with red claystones (MCl), and (9) oolitic dolostones (Do) (Figs. 3B–D, 4, 5).The characterization of the sedimentary facies from the dolomitic succession includes their composition, texture, sedimentary and /or biological structures among other important characteristics (Figs. 3, 4, 5).

4.2. Petrography

Dolostones are composed almost exclusively of dolomite (80–95%), other minerals identified in very low proportion were clays, siliceous cements and iron oxides. Dolomite crystals show variable degree of recrystallization from microcrystalline fabric-preserve to a completely fabric-destructive (Fig. 6B-F). The crystalline textures are represented by six types of dolomite (I –VI) useful for establishing the diagenetic evolution (e.g. Mountjoy and Amthor, 1994; Srinivasan et al., 1994; Wright, 1997).

4.2.1. Type I

Constituted by anhedral to subhedral dolomicrite crystals (2–15 μm) which conform a mosaic of non-planar xenotopic texture. This is the most common and representative in all studied sections (3:1), particularly forming stratiform and domical stromatolites Dl, Dbh and Dbe (Figs. 3F-I, 4, 6 B–C). Type I also constitutes the inner peloids and columnar stromatolites (<5 μm) (Fig. 6C), as well as inner rims of ooids (Fig. 6e). Under CL is dull and poor in iron.

4.2.2. Type II

This is typically a mosaic of planar euhedral rhombs (of 200–300 μm) with idiotopic texture (Fig. 6D). Some crystals show iron rich zonation with cloudy nuclei and clean rims constituting a sucrosic texture (Fig. 6E).

4.2.3. Type III

Characterized by rhombohedral dolomite crystals (200–300 μm) rich in Fe, with a prevalent planar-e or idiotopic texture. Iron distribution can originate well defined or diffuse layers (Fig. 6D), and constitutes the mottled and zebra dolomite.

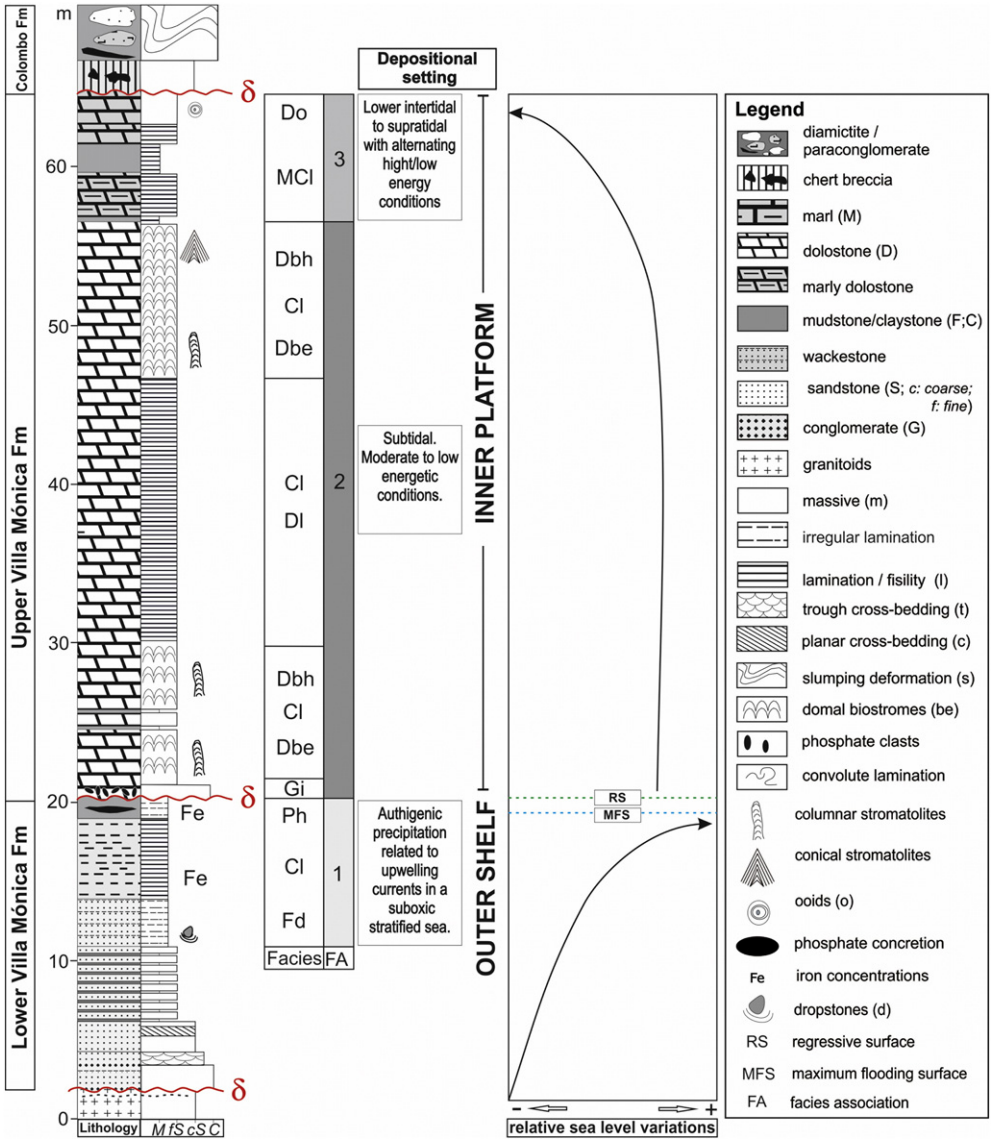

Fig. 5. Detailed section of Villa Mónica Formation (lower and upper sections) with additional paleoenvironmental interpretations and relative sea level variations. Abbreviations: FA: facies association; Fd: mudstone with dropstones; pH: phosphate lenses; Dbh: dolomitic domal bioherms; Dbe: dolomitic domical biostromes; Dl: laminated dolostones; Cl: laminated green claystones; CMl red laminated marls and claystones; Do: oolitic dolostone.

4.2.4. Type IV

This dolosparitic mosaic shows xenotopic texture of clean crystals variable in size (100–500 μm). This is associated to dissolution and reprecipitation of iron-rich dolomite, calcite filling up to 2 mm thick veins (Fig. 6F).

4.2.5. Type V

Constituted by anhedral saddle dolomite of 2 mm in size with sutured and serrated edges and undulant extinction, with a xenotopic non-planar texture and of clean crystals. This is infrequent and occasionally identified inner domical bioherms. A finer variety (500 μm to 1.5 mm), with planar-s hipidiotopic texture is recognized in patches.

4.2.6. Type VI

It is the less common, constituted by euhedral to subhedral crystlas growing in the walls-pores. This saddle dolomite display undulate extinction observed in the uppermost section near the karst (Fig. 6F).

4.3. Geochemistry

4.3.1. XRF and ICP analyses

Major element concentrations in dolostones (Colombo ~ Piedra Amarilla Quarry, COLD section) show average values of 28% CaO; 17% MgO; 7%SiO_2; 1.8% Fe_2O_3; 1%Al_2O_3; 0.6% K_2O; 0.2% Na_2O; TiO_2 0.1%; and MnO 0.08% in order of abundances (Table 1).

ICP-MS analyses of forty samples from the Tres Antenas and Colombo quarries (D, COLD and PA sections; Table 2) provide accurate Sr, Rb and Mn concentrations (Table 2). Sr concentrations vary from 22 to 83 ppm (Table 2) and Mn from 250 to 500 ppm (37 samples), while in the basal and upper sections exhibits Mn values >500 ppm (3 samples) and >1000 ppm (7 samples; Table 2). Most of these Mn and Sr values are similar to those reported for other Precambrian dolostones (Mn ~ 300 to 1200 ppm, and Sr 50 to 100 ppm; see Bartley et al., 2007). Mg/Ca is 0.7 in average (Table 2), indicative of stoichiometric dolomite in most cases, while Mn/Sr is <10 except for thirteen samples in which is >10 (Table 2). As postulated by Bartley et al. (2007) we consider that Mn/Sr < 10 may indicate "little altered" dolostones.

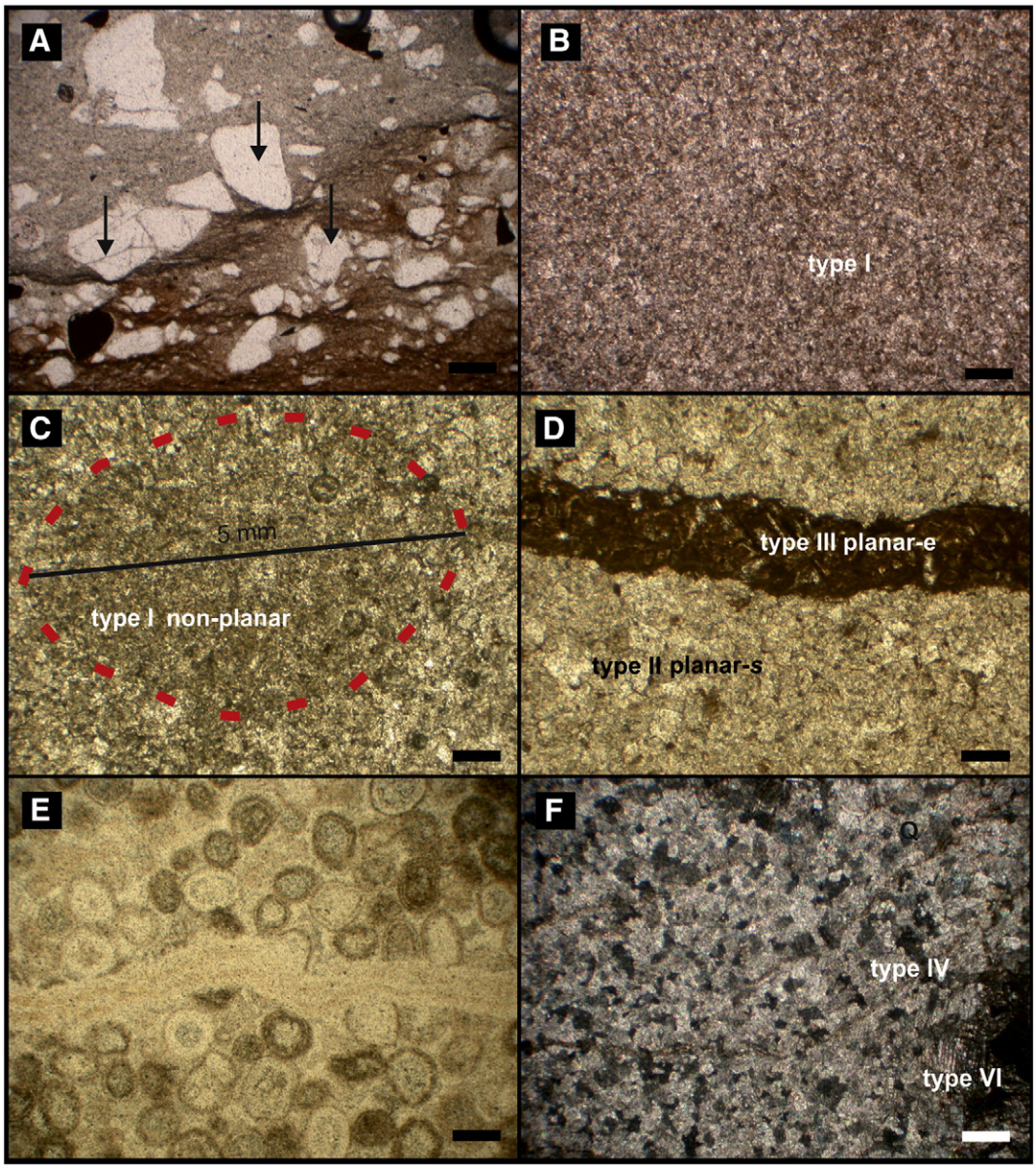

Fig. 6. Microphotographs from Villa Mónica Formation microfacies: (A) diamictite with dropstones = Fd; (B) dolomicrite of type I; C) type I (inner peloid); D) type II, and III as the fill of veins; (E) type I and II in ooids; (F) type IV with a pore with type VI (scale bar: 200 μm).

Rb values vary from 0.07 to 5.3, with one exception (17.5 ppm, sample TA 33 = marly dolostone). Rb/Sr values can be divided in two sets of samples: (1) conformed by nineteen samples with least altered Rb/Sr ratios (<0.01) ranging between 0.0016 and 0.0088, and (2) the other twenty samples (Rb/Sr > 0.01) which reach values from 0.03 to 0.52 (Table 2). Some authors indicate that Rb/Sr can be considered as primary when is lower than 0.001 in limestones and ≤0.01 in dolostones (Bartley et al., 2001; Delpomdor and Préat, 2013).

Rare-earth element + Y analyses (REY), from twenty-three samples, show total concentrations varying from ~ 3 to 54 ppm (Table 3). With one exception all samples show positive Eu anomalies (Table 3) that is regarded as a primary signal (Shields and Stille, 2001). All samples show slight positive Y anomalies (~0.70 to 1.30), whereas Y/Ho ratios are near PAAS values, of 31 in average and in all the cases ≤40. Gd shows positive anomaly in all samples with values of 1.22 in average. Three samples show LREE enrichment (Table 3), possibly reflecting inclusion of colloidal material that contained preferentially scavenged LREE from a nearby terrigenous input source (Notholt et al., 1989).

The VMF dolostones show a record of negative Ce anomalies varying from -0.4 to -1.8 (Table 3; Fig. 7). Ce anomaly may represent primary signature if no correlation with $La_N/Sm_N$is observed, with La_N/Sm_N ratios > 0.35 (McArthur and Walsh, 1984; Shields and Stille, 2001; Morad and Felitsyn, 2001). Most dolostones of the VMF fulfill this requirement (18 from 23 samples; see Table 3; Fig. 7A) and their composition may reflect paleoseawater redox conditions (Fig. 7A). According to different authors, if La is enriched negative Ce anomaly could be overestimated (Bau and Dulski, 1996; Shields and Stille, 2001; Chen et al., 2003). In order to assess the degree of La enrichment (Bau and Dulski, 1996; Webb and Kamber, 2000; Notholt et al., 1989), we find that Ce anomalies in most of the samples from VMF (11) show primary negative Ce anomalies, while Ce anomaly displayed by other ten samples is probably altered signal (Fig. 7B). The later could be explained as resulting of La_N enrichment related to Pr_N or Nd_N. Some complementary results obtained from previous work show the REE concentrations of the phosphates and shales from the underlying level (Table 3, Fig. 7A–B). From these results, a drastic change in the Ce anomalies

Table 1
Major element concentrations (wt%) of dolostone from the Colombo Quarry (COLD), Villa Mónica Formation.

	Lithology	Sample	CaO	Al_2O_3	Fe_2O_{3t}	MgO	SiO_2	Na_2O	K_2O	TiO_2	P_2O_5	MnO	LOI
Upper Villa Monica Formation	Dolostone	COLD 24	27.37	1.22	1.12	17.23	10.12	0.14	0.41	0.07	0.01	0.05	42.08
	Dolostone	COLD 23	28.48	0.72	1.14	17.40	8.54	0.00	0.25	0.05	0.01	0.05	28.88
	Dolostone	COLD 22	32.35	0.68	0.99	16.25	4.66	0.00	0.23	0.03	0.01	0.06	45.36
	Dolostone	COLD 21	30.31	1.08	1.22	17.26	5.18	0.00	0.37	0.06	0.01	0.06	44.37
	Dolostone	COLD 20	14.07	10.08	4.78	10.87	31.84	0.01	3.17	0.64	0.06	0.05	25.57
	Dolostone	COLD 19	20.74	5.40	3.36	14.24	19.98	0.00	1.79	0.32	0.04	0.07	35.19
	Dolostone	COLD 18	31.94	0.28	1.13	17.03	2.18	0.00	0.10	0.02	0.00	0.06	46.05
	Dolostone	COLD 17	27.83	1.63	1.20	16.93	7.12	0.00	1.75	0.09	0.01	0.05	42.33
	Dolostone	COLD 16	31.32	0.67	1.08	17.27	3.39	0.00	0.24	0.04	0.01	0.06	45.56
	Dolostone	COLD 15	31.27	0.68	1.00	16.64	4.57	0.00	0.24	0.04	0.01	0.05	45.9
	Dolostone	COLD 14	31.54	0.16	0.86	19.01	0.84	0.00	0.05	0.01	0.00	0.05	46.91
	Dolostone	COLD 13	31.16	0.48	0.72	18.91	0.76	0.00	0.16	0.04	0.01	0.05	47.37
	Dolostone	COLD 12	31.18	0.17	0.73	18.46	1.77	0.04	0.05	0.02	0.00	0.04	47.42
	Dolostone	COLD 11	31.07	0.64	0.95	18.35	1.35	0.00	0.20	0.06	0.04	0.05	46.91
	Dolostone	COLD 10	31.51	0.76	0.95	17.41	2.17	0.00	0.26	0.07	0.01	0.06	44.89
	Dolostone	COLD 9	30.21	0.57	1.06	18.20	2.33	0.03	0.21	0.05	0.01	0.07	45.40
	Dolostone	COLD 8	27.93	1.43	2.19	17.27	7.05	0.00	0.50	0.10	0.04	0.14	42.58
	Dolostone	COLD 7	28.47	1.32	1.87	18.13	4.73	0.00	0.46	0.10	0.03	0.08	43.34
	Dolostone	COLD 6	28.00	1.59	2.50	17.26	7.51	0.00	0.55	0.11	0.03	0.14	41.84
	Dolostone	COLD 5	27.79	1.73	2.63	16.94	7.27	0.01	0.59	0.12	0.03	0.14	41.81
	Dolostone	COLD 4	25.74	2.30	2.84	15.86	9.86	0.00	0.79	0.16	0.03	0.15	40.51
	Dolostone	COLD 3	27.55	2.10	2.56	16.74	5.97	0.09	0.66	0.14	0.04	0.16	42.31
	Dolostone	COLD 1	23.11	2.37	3.58	14.43	13.57	0.00	0.76	0.15	0.08	0.24	41.62

and Y/Ho mark a change in the seawater conditions from these two units (Table 3, Fig. 7).

4.3.2. Diagenesis evolution

Alteration related to process of dolomitization could be detected either petrographically, by textural features and/or presence of diagnostic minerals, or geochemically, through analysis of the behavior of some selected elements(e. g., Tucker, 1983; Knoll et al., 1986; Narbonne et al., 1994). Examples of geochemical correlations, used to identify altered samples and/or the degree of alteration of samples, are found in Marshall (1992), Wickham and Peters (1993), Kaufman and Knoll (1995), Jacobsen and Kaufman (1999), Melezhik et al. (2001) and Melezhik and Fallick (2003).

Trace-element content provides a powerful tool for assessing the degree of diagenesis. Sr, Mn, and Fe exhibit predictable behavior during alteration (e.g., Brand and Veizer, 1981; Veizer, 1983; Kah et al., 1999; Gómez Peral et al., 2007). In general, Sr content decreases through interaction with relatively Sr-poor fluids. Examination of Sr and Mn content in Villa Mónica dolostones, that are not related with$\delta^{18}O$ values (Fig. 8A-B), suggest that the principal control on Sr and Mn content is the mineralogy.

Assessment of Mn and Fe behavior in the context of mineralogy and fabric preservation is particularly useful (Fig. 8C). For dolostone samples, with fine-scale fabric preservation, Mn and Fe contents are relatively low (Table 2), compared with other older dolostones successions (Bartley et al., 2007).

Mn content typically increases with water–rock interaction in the presence of reduced fluids and therefore generally reflects either carbonate precipitation in the presence of Mn-rich waters (as might be expected in microbial mats), or post-depositional alteration under burial conditions. Most of the samples of dolostones contain350 to 620 ppm of Mn (thirty nine samples, Table 2), likely reflecting a combination of increased Mn mobility associated with microbial activity in peritidal environments and diagenesis by later fluids. Some samples show higher values of Mn (six, near 1000 ppm) and two, > 1800 ppm; however there is no correlation with $\delta^{18}O$ (Fig. 8B).

The analyzed dolostones show samples with expected Fe concentrations <10,000 ppm (eighteen samples) and others enriched in Fe (>10,000 ppm, five samples), again suggesting that samples retain different initial iron concentrations (Table 2; Fig. 8C-D).

Examining the relationship between Mn and Fe contents in the Villa Mónica dolostones, reveal a cluster of samples with lower Mn and Fe concentrations, and a scattering of points with Mn and Fe concentrations suggestive of significant enrichment in these elements (Kaufman and Knoll, 1995; Frank and Lyons, 2000, Fig. 8C). However, some samples enriched in Fe show low values in Mn (Fig. 8C). Even against such a background of moderate diagenesis, we expect that the fundamental character of a C-isotope curve might be retained. C-isotope composition is unrelated to Fe/Sr (Fig. 8E), Mn/Sr (Fig. 8F), or indicating that no carbon isotopic data should be rejected based on standard diagenetic criteria (Fig. 8E-F).

4.3.3. Chemostratigraphy

The carbon isotopic composition of dolostones (forty-three samples from Colombo, T3 and T6 sections) from Olavarría-Sierras Bayas area varies from ~−2 to +2.6‰, shows a trend to more positive values towards the top of this section (Table 2). $\delta^{18}O$ ranges from −0.5 to −7.5‰ in the three sections of this inner-platform dolostone (Table 2, Fig. 9).

The first isotope stratigraphic ^{13}C curve from dolostones of Villa Mónica Formation (seventeen results from Tres Antenas section) obtained by Gómez Peral et al. (2007) was interpreted as data altered by dolomitization processes. However, in the present work the integrated analysis of depositional conditions in which this rocks accumulated, added to a combination of chemical proxies (Mn, Sr, Rb, REE concentrations, etc.) allow to demonstrate the high degree of preservation of these rocks and consequently of the C and O isotopic results. Those data obtained from the Tres Antenas Quarry showed values of $\delta^{13}C$ from −1.36 to +2.20‰ and $\delta^{18}O$ from −2.1 to −6.5‰ (Gómez Peral et al., 2007; Table 2), which are highly correlated to the C—O isotope results from this work (Table 2). In addition, the same samples (from the Tres Antenas section) are now contrasted with results of Mn, Sr and Rb concentrations (Table 2) that are very similar to the other sections.

Dolostones immediately above the diamictite level (T3 and T6 of El Polvorín Quarry, Fig. 1B) show values of $\delta^{13}C$ from −1.31 to +2.58‰ and from −2.03 to +0.35‰ respectively, whereby the lowest value was found near the contact with the phosphate concretions at the basal section of the dolomitic section (Table 2). From base to top, the dolostones in general show increasing $\delta^{13}C$ values from −2 or −1‰ for the first fifteen meters (Table 2) and towards the top shows a narrow range between +1.7 up to +2.6‰ (Table 2). $\delta^{18}O$ show apparent correlation with $\delta^{13}C$ ratios (Table 2), but the weak correlation coefficient ($R^2 = 0.007$ in COLD, 0.26 in Tres Antenas, and 0.26 in PA sections) indicates that $\delta^{13}C$carb ratios are not altered significantly. On the other hand, they show moderate negative correlation in T3 and T6 sections from El Polvorín Quarry ($R^2 = 0.32$ and 0.64, respectively). Furthermore, $\delta^{13}C$

Table 2
C– and O– isotope and trace element composition of Villa Mónica dolostones from drill cores of El Polvorín Quarry (T3 and T6 sections), additional data from Tres Antenas Quarry in cursive (Gómez Peral et al., 2007).

	Sample	Lithofacies / environment	Microfacies	Height (m)	$\delta^{13}C_{carb}$ (‰ PDB)	$\delta^{18}O_{carb}$ (‰ PDB)	ICP-MS (ppm) Rb	Sr	Mn	Mn/Sr	Rb/Sr	Fe/Sr	Mg/Ca
Colombo Quarry	**COLD 25**	M-SD / SP	Types II–III	25	0.95	-4.56	0.8	30	1871	62.4	0.028	418	0.7
	COLD 24	M-SD / SP	Type II–III	24	0.36	-5.98	0.6	49	1194	24.4	0.012	183	0.7
	COLD 22	M-SD / SP	Type II–III	22	0.57	-7.48	0.5	57	1147	20.1	0.008	174	0.7
	COLD 20	SD / PR	Types I–II	20	0.65	-4.05	1.0	83	1055	12.7	0.012	111	0.7
	COLD 19	SD / PR	Types II–III	19	1.78	-4.04	7.9	47	1040	22.1	0.168	186	0.7
	COLD 18	LD / TF	Types I–II–III	18	0.54	-6.98	4.2	38	616	16.2	0.111	172	0.7
	COLD 17	LD / TF	Types I–II	17	0.55	-5.81	0.7	75	1070	14.3	0.009	102	0.7
	COLD 16	LD / TF	Types I–II	16	0.31	-6.14	1.1	72	508	7.1	0.016	52	0.7
	COLD 15	LD / TF	Types I–II	15	0.31	-6.56	0.5	48	439	9.1	0.010	69	0.8
	COLD 14	SD / PR	Type II	14	-0.34	-6.22	0.7	66	385	5.8	0.010	51	0.7
	COLD 13	SD / PR	Type II	13	-0.68	-5.82	0.2	39	339	8.7	0.006	65	0.7
	COLD 12	SD / PR	Type II	12	-0.56	-5.27	0.3	34	347	10.2	0.010	74	0.7
	COLD 11	SD / PR	Type II	11	-0.79	-5.83	0.2	35	362	10.3	0.006	86	0.7
	COLD 10	SD / PR	Type II	10	-0.93	-6.57	0.6	39	408	10.5	0.015	90	0.8
	COLD 9	SD / PR	Type II	9	-0.99	-5.72	0.5	68	424	6.2	0.007	56	0.8
	COLD 8	SD / PR	Type II	8	-1.2	-5.99	0.7	83	416	5.0	0.008	50	0.7
	COLD 7	SD / PR	Types I–II	7	-1.13	-5.85	1.2	63	485	7.7	0.018	63	0.8
	COLD 6	SD / PR	Types I–II	6	-1.32	-5.77	1.1	59	539	9.1	0.018	200	0.6
	COLD 5	SD / PR	Type II	5	-1.25	-5.74	1.2	46	416	9.0	0.027	364	0.6
	COLD 4	SD / PR	Type II	4	-1.59	-6.45	1.3	38	439	11.6	0.034	112	0.7
	COLD 3	SD / PR	Type II–III	3	-1.4	-3.46	1.9	46	431	9.4	0.042	75	0.8
	COLD 2	SD / PR	Type II	2	-1.3	-3.52	1.8	30	400	13.3	0.060	133	0.7
	COLD 1	SD / PR	Type II–III	0.01	-1.67	-3.86	1.7	60	393	6.5	0.028	65	0.7

	Sample	Lithofacies / environment	Microfacies	Depht (m)	$\delta^{13}C_{carb}$ (‰ PDB)	$\delta^{18}O_{carb}$ (‰ PDB)
T6 - El Polvorín Quarry	T6 - 4,3	LD / TF	Types I–II	4.3	0.35	-0.44
	T6 - 9,4	LD / TF	Types III–IV	9.4	-1.08	-7.46
	T6 - 13,5	LD / TF	Type I	13.5	-0.43	-5.29
	T6 - 15,8	LD / TF	Type I	15.8	-0.72	-5.53
	T6 - 25,5	SD / PR	Type I	25.5	-1.08	-7.06
	T6 26,05	SD / PR	Type I	26.05	-0.81	-5.98
	T6 - 27,6	SD / PR	Types I–II–III	27.6	-0.97	-6.09
	T6- 28,8	SD / PR	Types II–III	28.8	-1.32	-4.86
	T6- 32,6	M-SD / SP	Types II–III–IV	32.6	-2.03	-4.96

	Sample	Lithofacies / environment	Microfacies	Depht (m)	$\delta^{13}C_{carb}$ (‰ PDB)	$\delta^{18}O_{carb}$ (‰ PDB)
T3 - El Polvorín Quarry	T3-21,3	LD / TF	Types I–II	21.3	1.70	-3.52
	T3-23,7	LD / TF	Type III	23.7	1.89	-4.58
	T3-24,5	LD / TF	Types II–III	24.5	1.79	-3.69
	T3-31,3	LD / TF	Types I–II	31.3	2.58	-2.61
	T3-34,5	SD / PR	Types I–II	34.5	0.73	-6.39
	T3-37,95	SD / PR	Types I–II	37.95	0.44	-4.70
	T3-40,6	SD / PR	Types I–II	40.6	-0.07	-4.74
	T3-46,5	LD / TF	Types I–II	46.5	-0.23	-5.09
	T3-52,7	LD / TF	Types I–II	52.7	-0.57	-5.45
	T3-57,1	SD / PR	Types I–II	57.1	0.44	-4.70
	T3-66,1	SD / PR	Types II–III	66.1	-1.31	-6.13

	Sample	Lithofacies / environment	Microfacies	Height (m)	$\delta^{13}C_{carb}$ (‰ PDB)	$\delta^{18}O_{carb}$ (‰ PDB)	ICP-MS (ppm) Rb	Sr	Mn	Mn/Sr	Rb/Sr	Fe/Sr	Mg/Ca
Tres Antenas Quarry	**D 38**	M-SD / SP	Type I	30.78	*1.21*	*-3.33*	0.07	45	272	6.1	0.002	147	0.78
	D 37	M-SD / SP	Type I	29.29	*0.15*	*-2.11*							
	D 35`	M-SD / SP	Type II	26.78	*1.52*	*-3.93*							
	D 35	LD / TF	Type II	26.78	*1.46*	*-4.16*							
	D 33	LD / TF	Type I	24.78	*0.73*	*-2.60*	17.54	33	618	18.6	0.527	697	0.90
	D 31	LD / TF	Type II	22.28	*2.20*	*-4.98*	1.05	23	661	29.0	0.046	997	0.89
	D25	SD / PR	Type II				0.38	47	311	6.7	0.008	193	0.91
	D 21	SD / PR	Type II	18	*0.02*	*-5.97*	2.60	39	307	7.9	0.067	251	0.97
	D 20	SD / PR	Type II	17.2	*0.26*	*-5.43*	1.42	42	340	8.2	0.034	259	0.88
	D 20	SD / PR	Type II	17.2	*0.26*	*-5.57*	3.60	36	293	8.2	0.101	231	
	D 17	SD / PR	Type II	15.2	*0.22*	*-5.12*	1.81	39	342	8.7	0.046	269	0.93
	D 15	SD / PR	Type II	14	*-0.54*	*-4.59*		29	274	9.6		413	0.81
	D 13	SD / PR	Type II	12	*-0.03*	*-5.55*		22	288	13.2		357	1.00
	D 11	LD / TF	Type II	10	*-0.29*	*-6.49*		33	257	7.8		206	0.90
	D 09	LD / TF	Type II	8	*-0.65*	*-6.67*		38	250	6.6		189	0.90
	D 07	LD / TF	Type II	6	*-0.48*	*-6.14*		38	262	6.9			
	D 05	LD / TF	Types II–III				0.20	44	297	6.8	0.005	163	0.85
	D 03	LD / TF	Types II–III	2	*-0.58*	*-5.74*	1.49	48	2227	46.1	0.031		0.92
	D 01	LD / TF	Types II–III	0	*-0.49*	*-5.83*		42	302	7.3		147	0.90

	Sample	Lithofacies / environment	Microfacies	Height (m)	$\delta^{13}C_{carb}$ (‰ PDB)	$\delta^{18}O_{carb}$ (‰ PDB)	ICP-MS (ppm) Rb	Sr	Mn	Mn/Sr	Rb/Sr	Fe/Sr
Piedra Amarilla Quarry	**PA 25**	M-SD / SP	Types II–III	25	ni	ni	0.64	83	320	3.9	0.008	47
	PA 24	M-SD / SP	Type II–III	24	ni	ni	1.53	49	262	5.4	0.031	82
	PA 22	M-SD / SP	Type II–III	22	ni	ni	0.51	59	294	5.0	0.009	59
	PA 21	LD / TF	Types I–II	21	ni	ni	5.29	29	216	7.5	0.184	88
	PA 14	SD / PR	Types I–II	14	ni	ni		39	244	6.2		85
	PA 10	LD / TF	Types I–II	10	ni	ni	0.46	68	336	5.0	0.007	55
	PA 09	LD / TF	Types I–II	9	ni	ni	0.33	83	377	4.5	0.004	31
	PA 06	SD / PR	Types I–II	2.5	*-1.07*	*-5.10*						
	PA 05	SD / PR	Types I–II	2.5	*-1.08*	*-5.29*						
	PA 04	SD / PR	Types I–II	2	*-0.99*	*-5.64*						
	PA 03	SD / PR	Types I–II	1.5	*-0.27*	*-5.82*						
	PA 02	SD / PR	Types I–II	1	*-1.10*	*-5.47*						
	PA 011	SD / PR	Types I–II	0.5	ni	ni	0.07	45	272	6.1	0.002	147
	PA 01	SD / PR	Types I–II	0.5	*-1.36*	*-5.64*						
	PA 0	LD / TF	Types II–III	0	*-1.14*	*-5.25*						

Table 3
REE + Y analyses, Ce, Gd (ppm), Eu anomalies and elemental ratios for dolostones from the Tres Antenas and Colombo quarries (PA section).

		ICP-MS REE and Y (ppm)																					
	Sample	La	Ce	Pr	Nd	Sm	Eu	Gd	Tb	Dy	Y	Ho	Er	Tm	Yb	Lu	ΣREE	Gd anom	Ce anom	Eu anom	La/Sm	Ce/Ce*	Pr/Pr*	Y/Ho
Tres Antenas Quarry	D1	1.51	1.42	0.19	0.82	0.20	0.06	0.27	0.04	0.23	1.8	0.05	0.15	0.02	0.12	0.02	5.4	1.10	−1.60	1.26	1.09	0.59	1.02	35
	D3	1.35	15.46	2.11	8.68	2.18	0.52	2.62	0.35	1.97	12.1	0.38	1.06	0.14	0.84	0.12	40.4	1.18	−0.57	1.17	0.09	1.42	1.06	32
	D5	1.20	2.19	0.29	1.24	0.50	0.08	0.40	0.06	0.34	2.3	0.07	0.21	0.03	0.17	0.02	7.2	1.19	−1.42	1.52	0.79	0.85	1.03	34
	D7	1.35	1.45	0.18	0.74	0.19	0.05	0.25	0.03	0.21	1.6	0.04	0.12	0.02	0.10	0.01	5.0	1.50	−1.64	0.00	1.05	0.65	1.02	37
	D9	1.65	1.39	0.18	0.90	0.20	0.05	0.27	0.04	0.22	1.7	0.04	0.14	0.02	0.11	0.01	5.5	1.25	−1.56	1.26	1.20	0.55	0.91	38
	D11	0.70	0.88	0.11	0.49	0.16	0.05	0.19	0.02	0.16	1.2	0.03	0.10	0.01	0.07	0.01	3.2	1.35	−1.83	1.53	0.63	0.72	0.97	38
	D13	0.80	0.80	0.13	0.62	0.18	0.05	0.22	0.03	0.19	1.3	0.04	0.12	0.01	0.09	0.01	3.5	1.28	−1.73	1.33	0.66	0.56	1.05	35
	D15	1.45	2.03	0.55	2.69	0.75	0.20	0.95	0.13	0.71	4.0	0.14	0.39	0.05	0.30	0.04	11.2	1.15	−1.09	1.25	0.28	0.51	1.18	29
	D17	3.30	6.11	0.86	3.76	1.04	0.27	1.28	0.16	0.89	4.9	0.17	0.46	0.06	0.35	0.05	20.1	1.17	−0.92	1.27	0.46	0.84	1.03	29
	D20	5.03	4.82	0.64	2.78	0.74	0.18	0.91	0.12	0.67	3.8	0.13	0.35	0.04	0.27	0.04	17.7	1.19	−1.03	1.20	0.98	0.59	1.01	30
	D21	3.90	9.81	1.57	7.43	2.14	0.51	2.59	0.33	1.66	8.0	0.29	0.71	0.08	0.46	0.06	34.0	1.14	−0.62	1.19	0.26	0.88	1.04	28
	D25	3.63	8.15	1.10	4.39	1.04	0.25	1.30	0.16	0.89	5.0	0.18	0.50	0.06	0.40	0.06	23.5	1.27	−0.84	1.20	0.51	0.93	1.07	28
	D31	4.77	5.97	0.75	2.80	0.61	0.13	0.78	0.10	0.56	3.5	0.11	0.33	0.04	0.25	0.04	18.1	1.26	−1.01	1.03	1.13	0.72	1.07	31
	D33	2.97	6.77	1.13	5.20	1.55	0.41	2.26	0.32	1.78	8.6	0.34	0.92	0.12	0.70	0.10	26.6	1.08	−0.79	1.16	0.28	0.83	1.07	25
	D37	8.44	16.33	2.43	10.17	3.17	0.90	3.78	0.48	2.46	10.4	0.45	1.20	0.15	0.94	0.14	54.9	1.13	−0.43	1.41	0.39	0.83	1.09	23
Piedra Amarilla Quarry	PA1	6.71	1.69	0.23	0.94	0.23	0.06	0.31	0.04	0.27	1.8	0.05	0.16	0.02	0.13	0.02	11.2	1.25	−1.54	1.02	0.71	0.69	1.06	35
	PA9	4.97	9.36	1.26	5.13	1.29	0.32	1.61	0.20	1.09	6.6	0.20	0.54	0.06	0.37	0.05	28.1	1.22	−0.76	1.21	0.56	0.86	1.06	33
	PA10	4.23	7.40	1.04	4.16	1.10	0.28	1.34	0.17	0.97	5.9	0.19	0.52	0.07	0.40	0.05	23.3	1.19	−0.86	1.23	0.56	0.81	1.09	31
	P14	1.34	1.94	0.23	0.91	0.21	0.05	0.28	0.04	0.22	1.4	0.04	0.12	0.01	0.09	0.01	5.8	1.37	−1.55	1.07	0.92	0.80	1.01	34
	PA21	8.40	14.80	2.10	8.26	1.78	0.40	2.24	0.28	1.49	7.3	0.28	0.76	0.09	0.59	0.08	44.0	1.19	−0.52	1.12	0.69	0.81	1.11	26
	PA22	3.06	5.73	0.72	2.96	0.71	0.17	0.90	0.11	0.64	3.5	0.12	0.34	0.04	0.26	0.04	16.8	1.25	−1.02	1.16	0.63	0.89	1.03	28
	PA24	3.44	4.75	0.62	2.33	0.61	0.15	0.79	0.10	0.59	3.4	0.11	0.33	0.04	0.27	0.04	15.0	1.24	−1.11	1.20	0.82	0.75	1.09	30
	PA25	4.58	8.01	1.06	4.69	1.19	0.30	1.54	0.20	1.12	6.0	0.21	0.55	0.07	0.40	0.06	25.5	1.14	−0.81	1.19	0.56	0.84	1.01	29

PA section is comparable to COLD: the same locality.

vs. $\delta^{18}O$ diagram shows no relationship between sedimentary facies for example Dbh from the lower section shows $\delta^{13}C$of ~ −2‰ while in the upper section the same facies show positive $\delta^{13}C$ values up to ~+2‰ (Fig. 9).

5. Discussion

5.1. Paleoenvironmental evolution

Some paleoenvironmental considerations arise from the observation of the vertical distribution of the three facies associations (FAs) recognized between the end of the lower and the upper Villa Mónica Formation (VMF) (Figs. 4 and 5). At the last 10 m of lower VMF it is possible to recognize a FA that could be related to a glacial event supported by the presence of dropstones in clays, as previously interpreted by Gómez Peral et al. (2011, 2014). This FA is interpreted as developed in outer shelf settings, in a clear transgressive pattern, which contain a maximum flooding surface that promotes the authigenic precipitation of phosphate minerals as the result of minimal sedimentation rates. Over the lower VMF, the two FAs recognized in the upper VMF are related to a marine platform environment. FA2 includes an intraformational conglomerate with dolomitic marly matrix from the basal section of the unit, which is interpreted as the result of erosive regressive surface. It is important to note that, the time involving to the development of this surface was enough to generate phosphate pebbles, but not so long because there is a not clear age differentiation between lower and upper VMF (Gómez Peral et al., 2014). The rest of the FA2 is constituted by columnar, domical and stratified stromatolites (conforming biostromes and bioherms) and laminated dolostones, interbedded with thin levels of green claystones. The FA2 is interpreted as deposited in an intertidal to subtidal environment, in which minor changes of sea level and/or energy of the environment generate different stromatolitic morphologies (Serebryakov, 1976; Southgate, 1989; Poiré, 1993; Batten et al., 2004; Hoffman et al., 2012). Finally, the FA3 is constituted by interbedded reddish to purple marls with claystones (MCl), and oolitic dolostones (Do) on the top. The occurrence of terrigenous supply as well as the presence of ooids, can be interpreted as deposited in a shallowing upward trend, that grade from lower intertidal to higher energetic conditions into a supratidal setting (e.g., Jones and Derochers, 1992; Poiré, 1993; Wanless and Tedesco, 1993; Wright and Burchette, 1998; Batten et al., 2004; Hoffman et al., 2012), evidenced by tidal channels at the top.

In summary, from base to top, three main aspects should be highlighted: (1) a shift from siliciclastic to carbonate composition of the VMF; (2) a general transgression-regression pattern, which is evidenced by turning from an outer shelf to inner platform deposits; and (3) the existence of dolostones with large stromatolite communities especially the tubestone morphologies related to post-glacial cap carbonate (Corsetti and Grotzinger, 2015), could be considered as a clear evidence of a more favorable climatic conditions for the life (Wallace et al., 2015). All of these aspects will be deeper discussed below.

5.2. Dolomicrite and dolosparite origin

Dolomicrite constitutes the most common dolomite microtexture in stromatolitic and laminated dolostones of VMF. This dolomite type (I) was previously interpreted as the result of early dolomitization of calcite precursor (Poiré, 1987; Gómez Peral et al., 2007), as reported in other Neoproterozoic units (Zempolich et al., 1988; Zempolich and Baker, 1993; Gaucher et al., 2007). However, many authors reported that the very fine-grained nature of most dolomite implies that Neoproterozoic postglacial dolomite precipitated first as powder, possibly in the water column of the surface mixed layer before deposition and cementation (Riedgwell et al., 2003; Shields et al., 2007; Azmy et al., 2009). It is difficult to determine whether dolomite was the

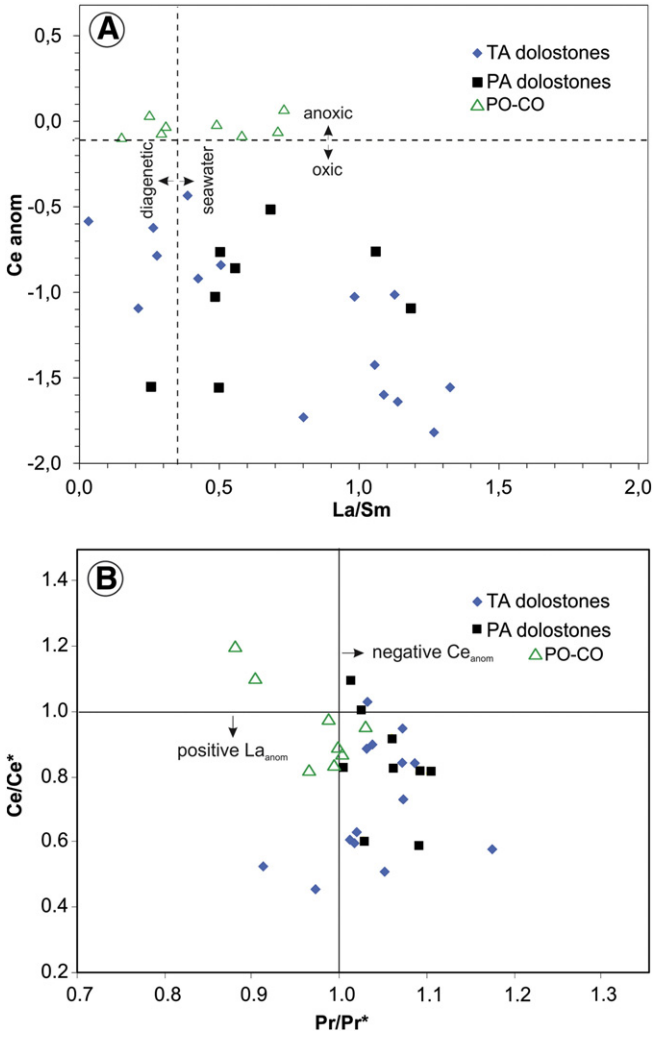

Fig. 7. A) Crossplot of Ce anomaly vs. La_N/Sm_N showing the distribution of dolomitic samples from Tres Antenas (TA) and Piedra Amarilla (PA) quarries. B) Ce/Ce* vs. Pr/Pr* diagram after Bau and Dulski (1996). This plot evaluates the possible overestimation of negative Ce anomalies due to La enrichment (>1.0 = three samples) in dolostones of the Villa Mónica Formation.

primary carbonate precipitate, but this possibility cannot be ruled out. In this case, primary dolomite could be constituted by dolomicrite (Fig. 6B–C). The saturation on dolomite of the ocean, which has been widely mentioned for Cryogenian successions, changed rapidly during and/or immediately following the deglaciation. This event is possibly developed within a short 10^3–10^4 year time frame of lithospheric relaxation, which is consistent with that envisaged in the Snowball-Earth Hypothesis (Hoffman et al., 1998, 2007; Hoffman and Schrag, 2002; Shields et al., 2007; Hood et al., 2011).

By contrast, the displacive growth of larger (<1 mm) dolomite crystals (Types II, III, and IV) within or in association with the dolomicrite speaks for substantial precipitation (cementation) of dolomite during diagenesis within the sediment, in many cases almost entirely replacing the original sediment.

Types II and III of dolomite are considered as aggradation of type I with typical planar-e textures (Fig. 6D), and internally can present alternation of rich and poor in iron dolomite. Ferrous dolomite is commonly associated with burial diagenesis indicating that type III represents an advanced stage of burial respect to type II. Also most of the stratified dolostones are constituted by types II and IV.

Types IV and V represent pervasive dolomitization by dissolution, replacement and recrystallization of the primary textures (Fig. 6F). Saddle dolomite is associated with deep burial dolomitization or as the product of interaction with later fluids (Tucker and Wright, 1990; Mountjoy and Amthor, 1994; Flügel, 2004).

5.3. REE–Y patterns

In order to determine whether the observed C isotopic compositions are likely to record a secular pattern of C isotopic change, we use other tools as microscopic analysis as well as REE–Y determinations. Numerous carbon isotopic studies have shown that stratigraphic $\delta^{13}C$ patterns are retained even with significant diagenesis (e.g., Fairchild et al., 1990; Kaufman et al., 1991; Frank and Lyons, 2000; Bartley et al., 2007).

The work of Banner et al. (1988) suggests that where diagenetic fluids and rocks have similar REE distributions, not being significantly changed by dolomitization. Hence, the difference between an assumed initial seawater-like REE signature in clean carbonates and the observed patterns in samples that have undergone extensive dolomitization or exposure to other mineralizing fluids may carry information about the chemistry, and possibly the source of those fluids (Nothdurft et al., 2004).

One indicator of preservation of the primary patterns is when the ΣREE concentrations are relatively low, and show no correlation with iron, regarding that the average concentrations in REE are near 20 ppm (Frimmel, 2009; Wang et al., 2014) (Table 3, Fig. 8d). Moreover, samples with higher Fe have similar REE concentrations (Fig. 8d), but in the Piedra Amarilla Quarry samples show lower Fe concentrations of 3800 ppm in average compared with those from Tres Antenas Quarry (~ 11,000 ppm in average; Table 3, Fig. 8d), suggesting that diagenetic Fe does not play a major role in controlling REE patterns.

It is important to highlight that the presence of negative Ce anomalies in dolostones, typical of seawater (Fig. 7b), is a good paleoredox indicator of the primary water body (Wright et al., 1987; Nothdurft et al., 2004; Frimmel, 2009).

The Y/Ho ratio in open seawater range typically between 44 and 90 but is strongly dependent on salinity (Lawrence et al., 2006). This makes the Y/Ho ratio a particularly useful monitor for the differentiation between marine and fresh water influenceddeposits (Bau, 1996; Nozaki et al., 1997; Nothdurft et al., 2004; Bolhar and Van Kranendonk, 2007; Wang et al., 2014). The Y/Ho ratios for almost all analyzed samples are within the range given for mixed seawater with fresh waters (≤40; Table 3).

5.4. Intrabasinal chemostratigraphic correlations

In order to better constrain the position of the VMF within the emerging Neoproterozoic carbon isotopic framework, we examined the isotopic characteristics of the known portions of the global curve. Dolostones are composed mainly by stoichiometric dolomite with Mg/Ca ≥ 0.6 (Table 2) also in agreement with X-ray determinations (Gómez Peral et al., 2007; Gómez Peral, 2008).The sedimentary isotopic records in this unit are considered near-primary because of the petrographic and geochemical proxies mentioned (Mn/Sr, REE, Ce anomalies), added to the $\delta^{18}O$, $\delta^{13}C$ values (Table 2; Figs. 8 and 9).

C and O-isotope chemostratigraphic curves compare variations from three sections of dolostones of the VMF (Fig. 9). They may be used for regional isotopic correlation and compared between all the studied sections. There is a clear positive trend in $\delta^{13}C$ upwards the dolomitic section of VMF. The predominant chemostratigraphic feature at this stratigraphic level is the presence of ^{13}C–depleted $\delta^{13}C$ values (−2 to 0‰) in the basal section, which shows similar trends to other reported in Cryogenian cap dolostones (Giddings and Wallace, 2009; Macdonald et al., 2010; Grey et al., 2011). These same authors indicate values showing excursions upwards of $\delta^{13}C$ up to +5‰ in those Cryogenian rocks, which are not recorded in Villa Mónica dolostones (≤+2.6‰). Taking into consideration that the $\delta^{13}C$ shows a positive trend upwards the VMF, we postulate that the most positive ^{13}C values can have been removed when the karstic surface eroded down the succession which

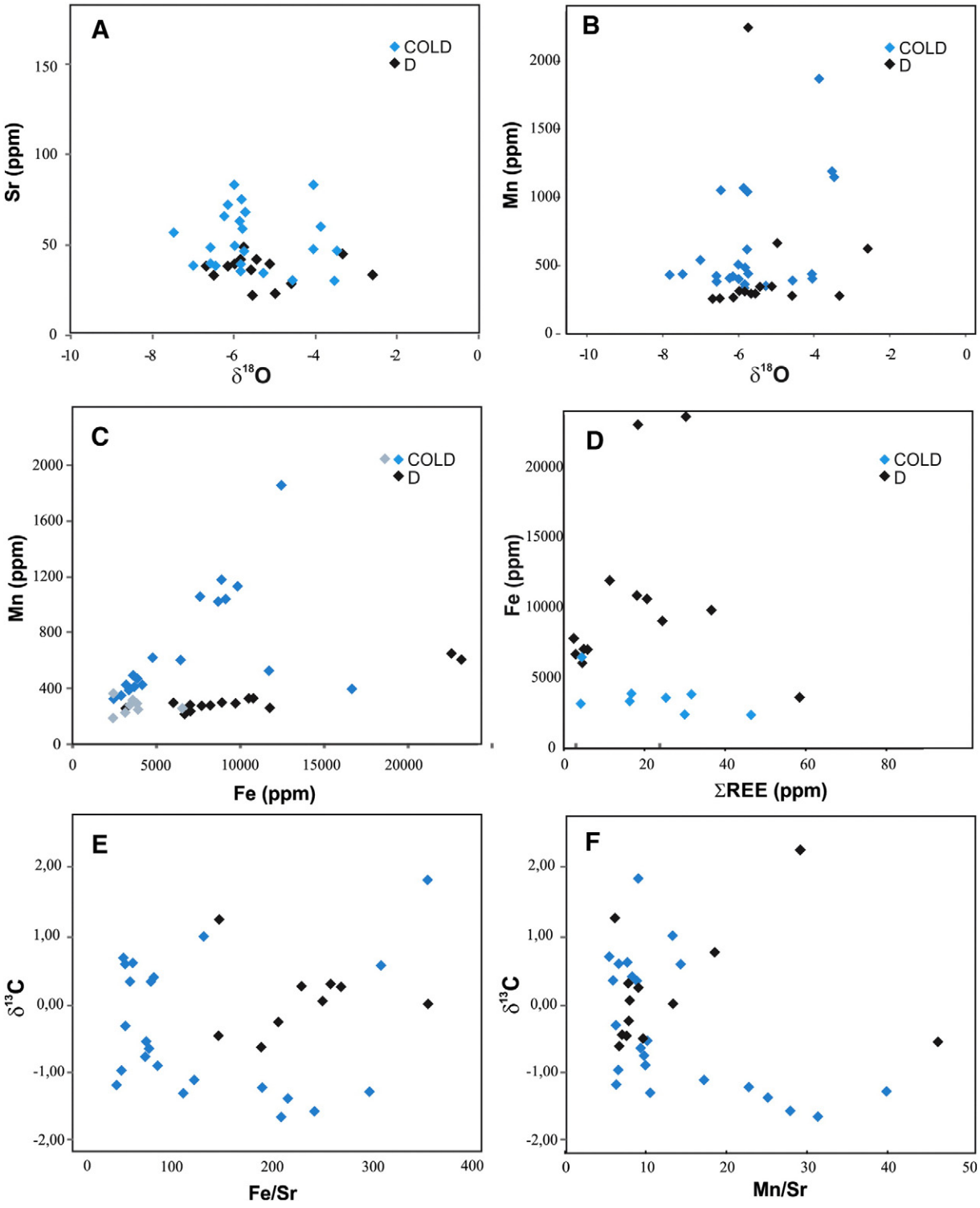

Fig. 8. Element concentrations versus isotope data for the Villa Mónica Formation: (A) Sr (ppm) vs. $\delta^{18}O$; (B) Mn (ppm) vs. $\delta^{18}O$; (C) Mn (ppm) vs. Fe (ppm); (D) Fe (ppm) vs $\sum$REE; E) $\delta^{13}C$ vs. Fe/Sr, and F) $\delta^{13}C$ vs. Mn/Sr.

is seen with reduced thickness (~40 m). Moreover, considering this carbonate platform could have been developed in a marginal setting of the Southwestern proto-Gondwana in which case VMF could represent and incomplete $\delta^{13}C$ record.

In addition, cap dolostones superseding Cryogenian glaciations show $\delta^{18}O$ (VPDB) values of −6 to −8‰, that are similar to the obtained for dolostones of VMF (−4 to −8‰; Table 2, Fig. 10), (Hoffman and Schrag, 2002), and distinctly lower than typical Neoproterozoic dolostones (Halverson et al., 2007).

Villa Mónica dolostones show widespread preservation of near primary microtextures (Types I and II; Fig. 6B, C and D) and less common textures related to moderate and local alteration (types III–VI; Fig. 6 F), with a consistent pattern of variation in carbon isotopic composition.

Although it is presently impossible to establish that the VMF and other Cryogenian cap-dolostones are coeval, they are likely to be broadly similar. These units exhibit a style of variation that suggests that the transition between predominantly 0‰ to positive values +2.6‰, suggestive of the post-glaciation steady state characterized by higher

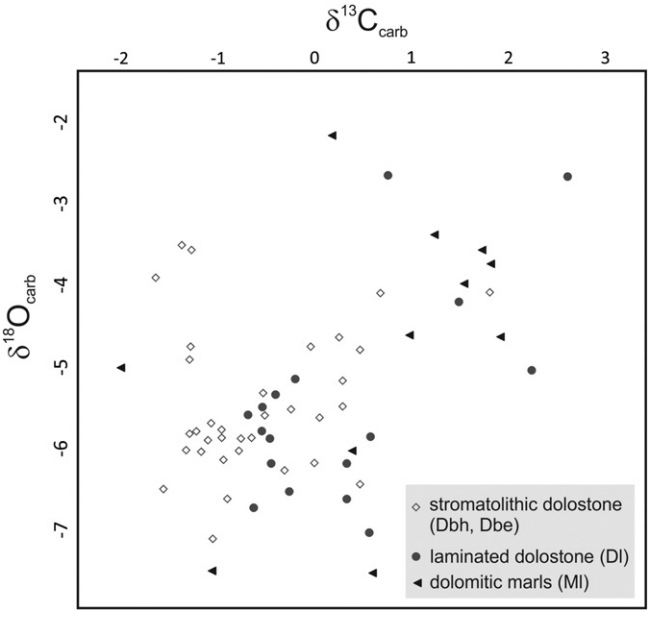

Fig. 9. $\delta^{13}C$ vs. $\delta^{18}O$ for the Villa Mónica dolostones. Notice the lack of correlation with the main dolomitic facies (see text for further discussion).

average $\delta^{13}C$ and greater isotopic variability, linked to global changes in carbon cycling and inorganic carbon reservoir size.

A rise in $^{87}Sr/^{86}Sr$ ratios from 0.7063 withinglacial deposits (Calver, 1998) to 0.7071 in interglacial succession (McKirdy et al., 2001) also compares closely with global records for Cryogenian dolostones. The Villa Mónica dolostones have relatively low and similar $^{87}Sr/^{86}Sr$ ratios (0.7068 to 0.7070; Gómez Peral et al., 2014), a feature interpreted as indication of near absence of post-depositional changes. Mn/Sr ratios <6 and $\delta^{18}O \geq -4.5‰$ reinforce that the Sr-isotope ratios should represent near-primary seawater isotopic values (Fig. 8A-B), also considering Rb/Sr obtained here of 0.0016 and 0.0078 respectively (samples PA11 and PA 25, Table 2).

Sr content in Villa Mónica dolostones is low (~50 ppm in average), in this regard it is known that Sr is systematically excluded from the tighter dolomite lattice structure during dolomitization, resulting in dolostones with lower Sr content than coeval limestone (Bartley et al., 2007). However, other authors suggest that higher Sr isotope values related to dolomitizationpoint to a detrital input orcontamination by diagenetic fluids (Demaiffe and Fieremans, 1981).

On the other hand, fresh water commonly presents low Sr contents (Brand and Veizer, 1981; Veizer, 1983), which is provided considerably during melt of ice sheets, decreasing the Sr from the sea in which dolostone platform develops. In agreement with that the precipitation of dolomite from mixed sea- and freshwater can explain the Sr-depleted fluids as the precursor of this dolomite Type I (Vahrenkamp and Swart, 1994; Azmy et al., 2001, 2009).

5.5. Paleoclimatic and paleonvironmental controls on chemostratigraphy

A comparison between REE and Y analyses of dolostones and phosphates (Gómez Peral et al., 2014), shows a drastic change in the Ce anomalies and Y/Ho that attest to a contrast in the seawater conditions from the two informal members of the lower and the upper Villa Mónica Formation (Table 3, Fig. 11).

The underlain phosphate level displays positive Ce anomalies (Fig. 7A–B; Gómez Peral et al., 2014), which make a contrast with the negative Ce anomalies registered in the upper dolostones in the present work (Fig. 11). This change can be associated with a progressive oxygenation and recirculation of seawater during implantation of the dolomitic platform related to an important sea level drop. This lithological boundary reflects a marked trend in $\delta^{13}C$ values from negative to positive as recorded in carbonates (e.g., Aharon et al., 1987; Banerjee et al., 1997; Mazumdar et al., 1999).

The phosphate level may have been precipitated under the effect of upwelling currents in a stratified sea (Gómez Peral et al., 2014). On the other hand, the dolomitic platform shows normal oxygen patterns, which can be associated with shallower setting. Then, if in deeper environment the sea was stratified, it cannot be told from the analyzed succession.

A considerable freshwater influence may be inferred for the depositional environments of these dolostones, those of the freshwater stromatolites from the VMF (Y/Ho < 30; Table 3). Continental deglaciation at the end of a glacial time would result in locally elevated freshwater levels in the platform with enhanced input of oxidants (i.e. O, NO_3^-) from the weathered continental crust (Svensen et al., 2004; Wang et al., 2014), which also may favors the primary precipitation of dolomicrite. Therefore, the oxygenated freshwater and brackish water environment should be as a response to the deglacial melt water input into the basin also reflected in low Sr contents of the dolomicrite analyzed.

As mentioned above, the basal portions of the VMF display negative $\delta^{13}C$ values that can be associated with cooler water conditions as was interpreted in other Neoproterozoic units (i.e. Halverson et al., 2007). This is supported by the presence of the underlaying mudstone with dropstones added to the postglacial phosphogenesis event recorded in the lower VMF (Gómez Peral et al., 2014). The shift to positive $\delta^{13}C$ values upwards (upper VMF) is in agreement with a climatic change to warmer conditions, consistent with the formation of the Sr-poor dolomite as the result of mixed melt- and seawater. Moreover, the increase in stromatolite biodiversity to the upper VMF reinforces the interpretation to more favorable climate conditions sustained by trends in $\delta^{13}C$.

Considering the sea-level changes, it is important to note that even when the upper VMF results from deposition during a post-glacial period, a considerable sea-level fall can be interpreted by the sedimentological data. This could be explaining, by the relationship between the eustatic variation and the isostatic rebound (Fig. 11). In this sense, during the final stage of deposition of the lower VMF, an early post-glacial scenario is the responsible of the generation of upwelling currents that results in the deposition of phosphates (Fig. 11). In this context, the eustatic positive variation is greater than the isostatic rebound generated by deglaciation, resulting in a relative sea-level rise. After that, acceleration in glacial-melt promotes an increase in the isostatic rebound, which highly exceeds the still positive eustacy, generating a marked regressive surface, and the beginning of the upper VMF. This change caused an important input of freshwater that contributes to the development of the dolomitic platform (Fig. 11). Finally, the interpretation of proximity to glacial areas is supported by different source of evidence (i.e. dropstones, chemical melt-water signatures, among other), but tillites or others unquestionable evidence have never been observed or mentioned in the study area.

6. Conclusions

The Villa Mónica dolostones, were previously framed between 1150 and 600 Ma, and represents the oldest sedimentary cover of the Río de La Plata Craton in Argentina, however shows very restricted post depositional alteration, as evidenced by preservation of primary dolomicrite microtexture.

In this basin-wide study of the Neoproterozoic Villa Mónica Formation (VMF) in Argentina, major and trace element proxies indicate a primary $\delta^{13}C$ signature reflected by different dolomitic facies, which show similar trends along all the studied sections in the Tandilia Basin. For that reason, $\delta^{13}C$ results previously interpreted as diagenetic overprinted needed to be reevaluated in the present work.

The negative $\delta^{13}C$ values characterize the contact between the dolostones and phosphate level (~−2‰), slightly higher ratios

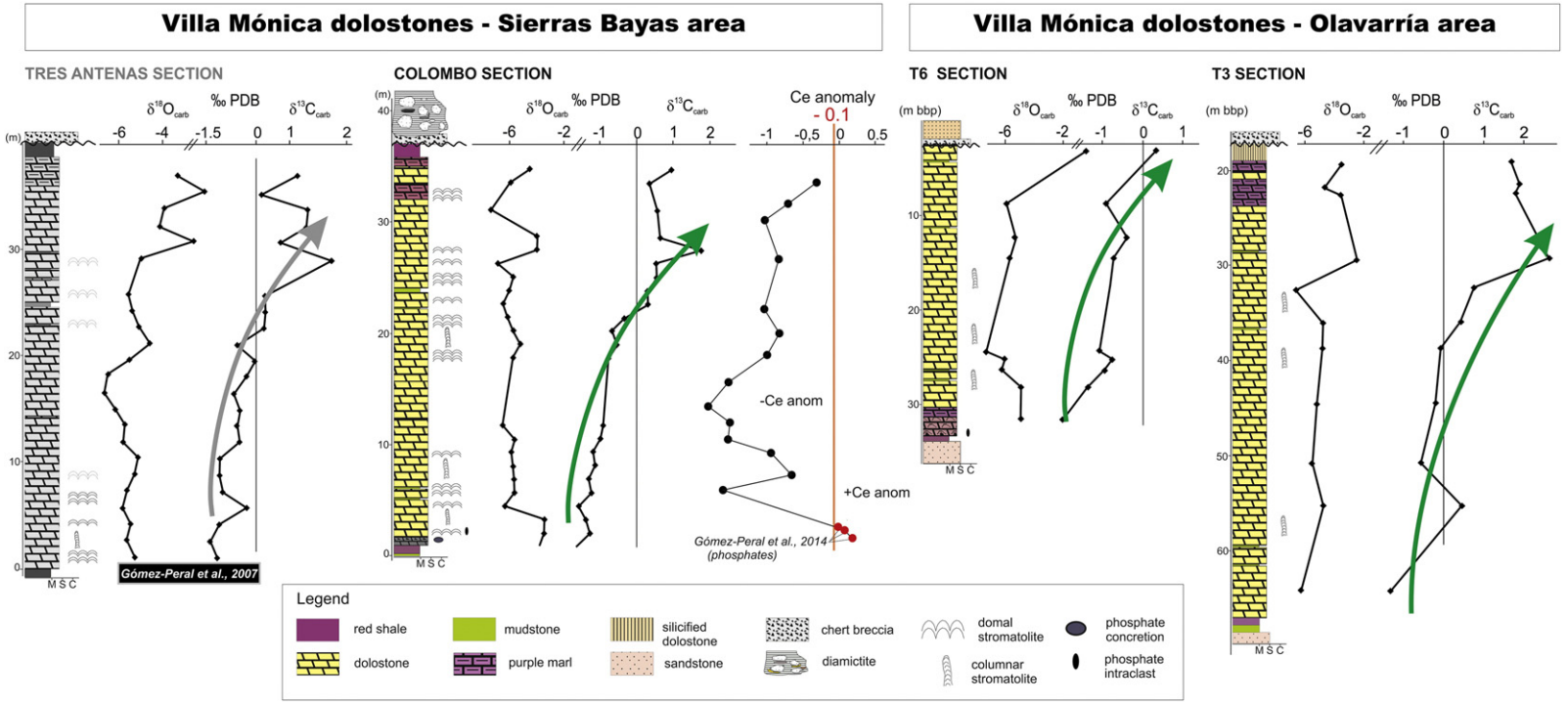

Fig. 10. Intrabasinal chemostratigraphic correlation between four sections of the Villa Mónica dolostones (Three from this work, and one from Gómez Peral et al., 2007). The arrows indicate the positive trend in $\delta^{13}C$ throughout the dolomitic facies succession. Ce anomalies are correlated in one section (Colombo Quarry).

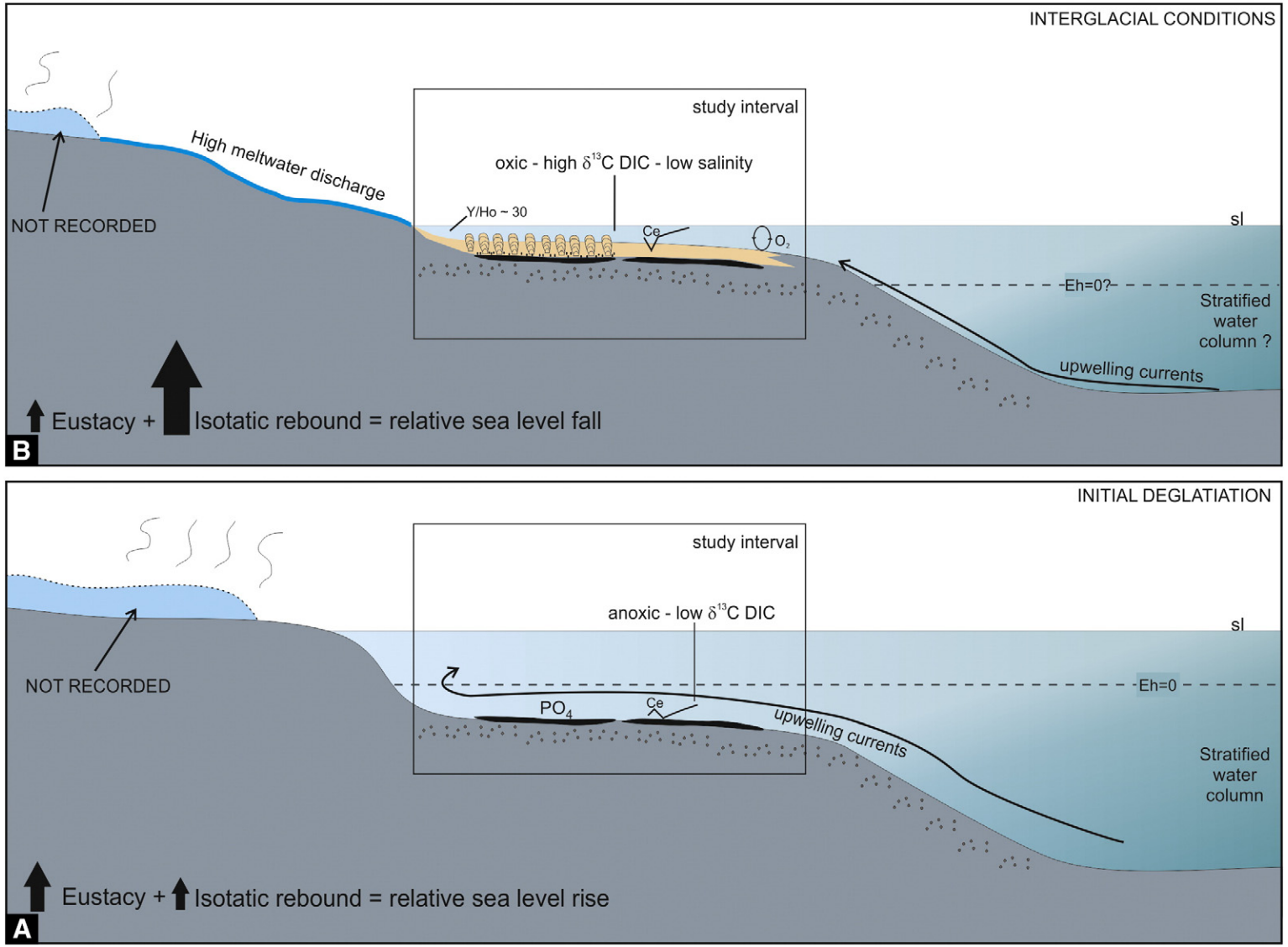

Fig. 11. Schematic representation to explain the trend in dissolved inorganic carbon (DIC) in $\delta^{13}C$, Ce anomalies related to redoxcline (Eh = 0) and seawater salinity. (a) Paleoenvironment scheme of the lower Villa Mónica Formation with a stratified basin during initial deglaciation related to low Eh (positive Ce anomaly) and negative $\delta^{13}C$. (b) Paleoenvironment scheme of the upper Villa Mónica Formation with normal circulation of oxygen leading to negative Ce anomalies and positive $\delta^{13}C$, associated with high meltwater discharge during an interglacial interval.

are predominant in the middle section of the dolomitic succession (from ~− 1‰ to 0‰), and turns to positive to the top of the sections (~+2.5‰). This pattern, added to unusually narrow range of non-radiogenic $^{87}Sr/^{86}Sr$ ~ 0.7068–0.7070, seems similar to that recorded for other Cryogenian tubestone-domianted dolomites known as typical morphologies from other post-Sturtian (~ 720 and 635 Ma) cap carbonates in Namibia, Brazil and western USA.

Positive $\delta^{13}C$ trends recorded and the increase in stromatolite biodiversity are linked to the buildup of oxygen in association to a global warming, which expression is the expected for this marginal position of the southwestern proto-Gondwana basin.

The predominance of dolomite of type I in the stromatolitic dolomite facies studied could be in agreement with required alkalinity typical from *syn*-glacial ocean as well as the expected rise in Sr poor meltwater included in the initial dolomite mineral.

We found that Villa Mónica dolostones retained their original seawater-melt water REY patterns in samples that also preserve their near original texture and mineralogy. Overall, the $\sum$ REY contents in samples as expected are very scarce (~20 ppm in average). In addition, the dolostones from VMF meet all of these requirements that ascribed to a seawater origin under oxic conditions. In this sense, the change from positive (phosphates) to negative Ce anomalies (dolostones), constitutes an evidence of a change in the sea redox conditions from a stratified ocean (outer shelf) to a well-oxygenated (dolomitic inner platform) water column.

Finally, the regression marked by the contact between the lower siliciclastic VMF with the upper dolomitic VMF is linked to a $\delta^{13}C$ positive trend upwards and supports the connection between dolomite precipitations, high melt-water input in a proximity to a glacial area. Such an interpretation matches the emerging consensus and evidence from the Tandilia Basin was in a marginal setting on the continents during the breaking of Rodinia to the configuration of Gondwana in which Neoproterozoic glaciations were poorly represented.

Acknowledgements

We are especially grateful to José M. Canallichio (Cementos Avellaneda S.A.), to D. Mártire for the preparation of thin sections, and C. Cavarozzi and M. Pedemonte for the ICP-MS analysis; and to G. Casal for English review. Prof. C. Gaucher is also thanked for comments and suggestions that helped improving our original manuscript. Field work and laboratory materials were supported by grants to LEGP (projects PIP-0134 and PICT Pres. BID 2012-2798) and laboratory analyses by grants to A.N. Sial (CNPq 470399/2008, CNPq 472842/2010-2, and FACEPE APQ 0727-1.07/08). This is the NEG-LABISE contribution n. 266. The authors specially thank the anonymous reviewer and the Editor B. Jones for their very constructive reviews.

References

Aharon, P., Schidlowski, M., Singh, I.B., 1987. Chronostratigraphic markers in the end-Precambrian carbon isotope record of the Lesser Himalaya. Nature 327, 699–701.

Alvarenga, C.J.S., Santos, R.V., Vieira, L.C., Lima, B.A.F., Mancini, L.H., 2014. Meso-Neoproterozoic isotope stratigraphy on carbonates platforms in the Brasilia Belt of Brazil. Precambrian Research 251, 164–180.

Arrouy, M.J., Poiré, D.G., Gómez Peral, L.E., Canalicchio, J.M., 2015. Sedimentología y estratigrafía del grupo La Providencia (Nom. Nov.): Cubierta Neoproterozoica, Sistema de Tandilia, Argentina. Latin American Journal of Sedimentology and Basin Analysis 22 (2), 1–38.

Arrouy, M.J., Warren, L.V., Quaglio, F., Poiré, D.G., Guimarães Simões, M., Boselli, M.R., Gómez Peral, L.E., 2016. Ediacaran discs from South America: probable soft-bodied macrofossils unlock the paleogeography of the Clymene Ocean. Scientific Reports 6 (30590):1–10. http://dx.doi.org/10.1038/srep30590.

Azmy, K., Veizer, J., Misi, A., de Oliveira, T.F., Lima Sanches, A., Dardenne, M.A., 2001. Dolomitization and isotope stratigraphy of the Vazante Formation, Sao Francisco Basin, Brazil. Precambrian Research 112, 303–329.

Azmy, K., Sylvester, P., de Oliveira, T.F., 2009. Oceanic redox conditions in the Late Mesoproterozoic recorded in the upper Vazante Group carbonates of São Francisco Basin, Brazil: evidence from stable isotopes and REEs. Precambrian Research 168, 259–270.

Banerjee, D.M., Schidlowski, M., Siebert, F., Brasier, M.D., 1997. Geochemical changesacross the Proterozoic–Cambrian transition in the Durmala phosphorite minesection, Mussoorie Hills, Garhwal Himalaya, India. Palaeogeography, Palaeoclimatology, Palaeoecology 132, 183–194.

Banner, J.L., Hanson, G.N., Meyers, W.J., 1988. Rare earth element and Nd isotopic variations in regionally extensive dolomites from the Burlington-Keokuk Formation (Mississippian): implications for REE mobility during carbonate diagenesis. Journal of Sedimentary Petrology 58, 415–432.

Bartley, J.K., Semikhatov, M.A., Kaufman, J.A., Knoll, A.H., Pope, M.C., Jacobsen, S.B., 2001. Global events across the Mesoproterozoic– Neoproterozoic boundary: C and Sr isotopic evidence from Siberia. Precambrian Res. 111, 165–202.

Bartley, J.K., Kah, L.C., McWilliams, J.L., Stagner, A.F., 2007. Carbon isotope chemostratigraphy of the middle Riphean type section (Avzyan formation, southern Urals, Russia): signal recovery in a fold-and-thrust belt. Chemical Geology 237, 211–232.

Batten, K.L., Narbonne, G.M., James, N.P., 2004. Paleoenvironments and growth of early Neoproterozoic calcimicrobial reefs: platformal Little Dal Group, northwestern Canada. Precambrian Research 133, 149–169.

Bau, M., 1996. Controls on the fractionation of isovalent trace elements in magmatic and aqueous systems: evidence from Y/Ho, Zr/Hf, and lanthanide tetrad effect. Contributions to Mineralogy and Petrology 123 (3), 323–333.

Bau, M., Dulski, P., 1996. Distribution of yttrium and rare-earth elements in the Pengeand Kuruman iron-formations, Transvaal Suergroup, South Africa. Precambrian Research 79, 37–55.

Bennett, M.R., Doyle, P., Mather, A.E., 1996. Dropstones: their origin and significance. Palaeogeography Palaeoclimatology Palaeoecology 121, 331–339.

Bolhar, R., Van Kranendonk, M.J., 2007. A non-marine depositional setting for the northern Fortescue Group, Pilbara Craton, inferred from trace element geochemistry of stromatolitic carbonates. Precambrian Research 155, 229–250.

Bonhomme, M.G., Cingolani, C.A., 1980. Mineralogía y geocronología Rb-Sr y K-Ar de fracciones finas de la "Formación La Tinta", Provincia de Buenos Aires. Revista de la Asociación Geológica Argentina 35 (4), 519–538.

Brand, U., Veizer, J., 1981. Chemical diagenesis of multicomponent carbonate system — 2: stable isotopes. Journal of Sedimentary Petrology 51, 987–997.

Brasier, M.D., Shields, G.A., 2000. Chemostratigraphy and correlation of the Neoproterozoic Port Askaig glaciation, Dalradian Supergroup of Scotland. Journal of the Geological Society (London) 157, 909–914.

Calver, C.R., 1998. Isotope stratigraphy of the Neoproterozoic Togari Group, Tasmania. Australian Journal of Earth Sciences 45 (6), 865–874.

Chen, D.F., Dong, W.Q., Qi, L., Chen, G.Q., Chen, X.P., 2003. Possible REE constraints onthe depositional and diagenetic environment of Doushantuo Formation phosphorites containing the earliest metazoan fauna. Chemical Geology 201, 103–118.

Cingolani, C., 2011. The Tandilia System of Argentina as a southern extension of the Río de la Plata craton: an overview. International Journal of Earth Sciences 100, 221–242.

Cingolani, C., Bonhomme, M.G., 1988. Resultados geocronológicos en niveles pelíticos intercalados en las dolomías de Sierras Bayas (Grupo La Tinta), provincia de Buenos Aires. Segundas Jornadas Geológicas Bonaerenses. Buenos Aires, Argentina, pp. 283–289.

Cingolani, C.A., Hartmann, L.A., Santos, J.O.S., McNaughton, N.J., 2002. U–Pb SHIMP dating of zircons from the Buenos Aires Complex of the Tandilia Belt, Rio de La Plata Craton, Argentina. Actas XV Congreso Geológico Argentino, El Calafate.

Cloud, P., Dardenne, M., 1973. Proterozoic age of the Bambuí Group in Brazil. Geological Society of America Bulletin 84 (5), 1673–1676.

Corkeron, M., 2007. 'Cap carbonates' and Neoproterozoic glacigenic successions from the Kimberley region, north-west Australia. Sedimentology 54, 871–903.

Corsetti, F.A., Grotzinger, J.P., 2015. Origin and Significance of Tube Structures in Neoproterozoic Post-glacial Cap Carbonates: Example from Noonday Dolomite, Death Valley, United States. Geology 43 (5), 459–462.

Delpomdor, F., Préat, A., 2013. Early and late Neoproterozoic C, O and Sr isotope chemostratigraphy in the carbonates of West Congo and Mbuji-Mayi supergroups: A preserved marine signature? Palaeogeography, Palaeoclimatology, Palaeoecology 389 (2013), 35–47.

Demaiffe, D., Fieremans, M., 1981. Strontium-isotopic geochemistry of the Mbuji-Mayi and Kundelungu kimberlites (Zaire, Central Africa). Chemical Geology 31, 311–323.

Dickson, J.A.D., 1966. Carbonate identification and genesis as revealed by staining. Journal of Sedimentary Petrology 36, 491–505.

Elderfield, H., Graves, M.J., 1982. The Rare earth elements in sea water. Nature 296, 214–219.

Fairchild, I.J., Marshall, J.D., Bertrand-Sarfati, J., 1990. Stratigraphic shifts in carbon isotopes from Proterozoic stromatolitic carbonates (Mauritania): influences of primary mineralogy and diagenesis. American Journal Science 290-A, 46–79.

Flügel, E., 2004. Microfacies of Carbonate Rocks; Analysis, Interpretation and Application. Springer-Verlag, Berlin (976 pp.).

Frakes, L.A., Francis, J.E., 1988. A guide to Phanerozoic cold polar climates from high-latitude ice-rafting in the Cretaceous. Nature 333, 547–549.

Frank, T.D., Lyons, T.W., 2000. The integrity of $\delta^{18}O$ records in Precambrian carbonates: a Mesoproterozoic case study. In: Grotzinger, J.P., James, N.P. (Eds.), SEPM Carbonate Sedimentation and Diagenesis in the Evolving Precambrian World. (Society for Sedimentary Geology) Special Publication vol. 65, pp. 315–326 (Tulsa).

Frimmel, H.E., 2009. Trace element distribution in Neoproterozoic carbonates as palaeoenvironmental indicator. Chemical Geology 258, 338–353.

Gaucher, C., Poiré, D., 2009. Biostratigraphy. Neoproterozoic-Cambrian evolution of the Río de la Plata Palaeocontinent. In: Gaucher, C., Sial, A.N., Halverson, G.P., Frimmel, H.E. (Eds.), Neoproterozoic–Cambrian Tectonics, Global Change and Evolution: A Focus on Southwestern Gondwana. Developments in Precambrian Geology 16. Elsevier, pp. 103–114.

Gaucher, C., Poiré, D.G., Gómez-Peral, L.E., Chiglino, L., 2005. Litoestratigrafía, bioestratigrafía y correlaciones de las sucesiones sedimentarias del Neoproterozoico-Cámbrico del Cratón del Río de La Plata (Uruguay y Argentina). Latin American Journal of Sedimentology and Basin Analysis 12 (2), 145–160.

Gaucher, C., Sial, A.N., Ferreira, V.P., Pimentel, M.M., Chiglino, L., Sprechmann, P., 2007. Chemostratigraphy of the Cerro Victoria Formation (Lower Cambrian, Uruguay): evidence for progressive climate stabilization across the Precambrian- Cambrian boundary. Chemical Geology 237, 28–46.

Gaucher, C., Finney, S.C., Poiré, D.G., Valencia, V.A., Grove, M., Blanco, G., Pamoukaghlián, K., Gómez Peral, L., 2008. Detrital zircon ages of Neoproterozoic sedimentary successions in Uruguay and Argentina: insights into the geological evolution of the Río de la Plata Craton. Precambrian Research 167, 150–170.

Giddings, J.A., Wallace, M.W., 2009. Facies-dependent $\delta^{13}C$ variation from a Cryogenian platform margin, South Australia: evidence for stratified Neoproterozoic oceans? Palaeogeography, Palaeoclimatology, Palaeoecology 271, 196–214.

Gómez Peral, L.E., 2008. Petrología y diagénesis de las unidades sedimentarias precámbricas de Olavarría, Provincia de Buenos Aires. (Tesis doctoral). Facultad de Ciencias Naturales y Museo, Universidad Nacional de La Plata (Tomo I: 327pp y tomo II: 292 pp. (online SEDICI-UNLP)).

Gómez Peral, L.E., Poiré, D.G., Strauss, H., Zimmermann, U., 2007. Chemostratigraphy and diagenetic constraints on Neoproterozoic carbonate successions from the Sierras Bayas Group, Tandilia System, Argentina. Chemical Geology 237, 127–146.

Gómez Peral, L.E., Raigemborn, M.S., Poiré, D.G., 2011. Petrología y evolución diagenética de las facies silicoclásticas del Grupo Sierras Bayas, Sistema de Tandilia, Argentina. Latin American Journal of Sedimentology and Basin Analysis (LAJSBA) 18 (1), 3–41.

Gómez Peral, L.E., Kaufman, A.J., Poiré, D.G., 2014. Paleoenvironmental implications of two phosphogenic events in Neoproterozoic sedimentary successions of the Tandilia System, Argentina. Precambrian Research 252, 88–106.

Grey, K., Hill, A.C., Calver, C., 2011. Biostratigraphy and stratigraphic subdivision of Cryogenian successions of Australia in a global context. In: Arnoud, E., Halverson, G.P., Shields-Zhou, G. (Eds.), The Geological Record of Neoproterozoic Glaciations. Geological Society, London, Memoirs 36 (1), pp. 113–134.

Halverson, G.P., Maloof, A.C., Schrag, D.P., Dudas, F.O., Hurtgen, M.T., 2007. Stratigraphy and geochemistry of a ca. 800 Ma negative carbon isotope interval in northeastern Svalbard. Chemical Geology 237, 5–27.

Halverson, G.P., Wade, B.P., Hurtgen, M.T., Barovich, K.M., 2010. Neoproterozoic chemostratigraphy. Precambrian Research 182, 337–350.

Hill, A.C., Cotter, K.L., Grey, K., 2000. Mid-Neoproterozoic biostratigraphy and isotope stratigraphy in Australia. Precambrian Research 100, 281–298.

Hoffman, P.F., Schrag, D.P., 2002. The snowball Earth hypothesis: testing the limits of global change. Terra Nova 14, 129–155.

Hoffman, P.F., Kaufman, A.J., Halverson, G.P., Schrag, D.P., 1998. A Neoproterozoic snowball Earth. Science 281, 1342–1346.

Hoffman, P.F., Halverson, G.P., Domack, E.W., Husson, J.M., Higgins, J.A., Schrag, D.P., 2007. Are basal Ediacaran (635 Ma) post-glacial "cap dolostones" diachronous? Earth and Planetary Science Letters 258, 113–131.

Hoffman, P.F., Halverson, G.P., Domacke, E.W., Malooff, A.C., Swanson-Hysellf, N.L., Cox, G.M., 2012. Cryogenian glaciations on the southern tropical paleomargin of Laurentia (NE Svalbard and East Greenland), and a primary origin for the upper Russøya (Islay) carbon isotope excursion. Precambrian Research 206–207, 137–158.

Hood, A.v.S., Wallace, M.W., Drysdale, R.N., 2011. Neoproterozoic aragonite-dolomite seas? Widespread marine dolomite precipitation in Cryogenian reef complexes. Geology 39, 871–874.

Iñiguez Rodríguez, A.M., 1999. La Cobertura Sedimentaria de Tandilia. In: Caminos, R. (Ed.), Geología Argentina. SEGEMAR, pp. 101–106.

Jacobsen, S.B., Kaufman, A.J., 1999. The Sr, C and O isotopic evolution of Neoproterozoic seawater. Chemical Geology 161, 37–57.

Johansson, A., 2014. From Rodinia to Gondwana with the 'SAMBA' model—a distant view from Baltica towards Amazonia and beyond. Precambrian Research 244, 226–235.

Jones, B., Desrochers, A., 1992. Shallow Platform Carbonates. In: Walker, R.G., James, N.P. (Eds.), Facies Models: Response to Sea Level Changes. Geol. Ass. Can., pp. 277–301.

Kah, L.C., Sherman, A.G., Narbonne, G.M., Knoll, A.H., Kaufman, A.J., 1999. $\delta^{13}C$ stratigraphy of the Proterozoic Bylot Supergroup, Baffin Island, Canada: implications for regional lithostratigraphic correlations. Canadian Journal of Earth Sciences 36, 313–332.

Kaufman, A.J., Knoll, A.H., 1995. Neoproterozoic variations in the C-isotopic composition of seawater; stratigraphic and biogeochemical implications. Precambrian Research 73, 27–49.

Kaufman, A.J., Hayes, J.M., Knoll, A.H., Germs, G.J.B., 1991. Isotopic compositions of carbonates and organic carbon from upper Proterozoic successions in Namibia: stratigraphic variation and the effects of diagenesis and metamorphism. Precambrian Research 49, 301–327.

Kaufman, A.J., Knoll, A.H., Narbonne, G.M., 1997. Isotopes, ice ages, and terminal Proterozoic Earth history. PNAS, Proceedings of the National Academy of Sciences of the United States of America 94, 6600–6605.

Kaufman, A.J., Sial, A.N., Frimmel, H.E., Misi, A., 2009. Neoproterozoic to Cambrian palaeoclimatic events in southwestern Gondwana. In: Gaucher, C., Sial, A.N., Halverson, G.P., Frimmel, H.E. (Eds.), Neoproterozoic–Cambrian Tectonics, GlobalChange and Evolution: A Focus on Southwestern Gondwana. Developments in Precambrian Geology vol. 16. Elsevier, pp. 369–388.

Kawashita, K., Varela, R., Cingolani, C., Soliani Jr., E., Linares, E., Valencio, S.A., Ramos, A.V., Do Campo, M., 1999. Geochronology and Chemostratigraphy of "La Tinta" Neoproterozoic Sedimentary rocks, Buenos Aires Province, Argentina. II South American Symposium on Isotope Geology. Brazil, pp. 403–407.

Kennedy, M.J., Runnegar, B., Prave, A.R., Hoffmann, K.-H., Arthur, M.A., 1998. Two or four Neoproterozoic glaciations? Geology 26, 1059–1063.

Knoll, A.H., Swett, K., Mark, J., 1991. The Draken Conglomerate Formation: paleobiology of a Proterozoic tidal flat complex. Journal of Paleontology 65, 531–569.

Knoll, A.H., Walter, M.R., Narbonne, G.M., Christie-Blick, N., 2006. The Ediacaran Period: a new addition to the geologic time scale. Lethaia 39, 13–30.

Knoll, A.H., Hayes, J.M., Kaufman, A.J., Swett, K., Lambert, I.B., 1986. Secular variation in carbon isotope ratios from Upper Proterozoic successions of Svalbard and East Greenland. Nature 321, 832–838.

Lawrence, M.G., Kenneth, A.G., Collerson, D., Kamber, B.S., 2006. Direct quantification of rare earth element concentrations in natural waters by ICP-MS. Applied Geochemistry 21, 839–848.

Macdonald, F.A., Schmitz, M.D., Crowley, J.L., Roots, C.F., Jones, D.S., Maloof, A.C., Strauss, J.V., Cohen, P.A., Johnson, D.T., Schrag, D.P., 2010. Calibrating the Cryogenian. Science 327, 1241–1243.

Marshall, J.D., 1992. Climatic and oceanographic isotopic signals from the carbonate record and their preservation. Geological Magazine 129, 143–160.

Mazumdar, A., Banerjee, D.M., Schidlowski, M., Balaram, V., 1999. Rare-earth ele-ments and stable isotope geochemistry of early Cambrian chert-phosphorite assemblages from the lower Tal formation of the Krol Belt (lesser Himalaya,India). Chemical Geology 156, 275–279.

McArthur, J.M., Walsh, J.N., 1984. Rare-earth element geochemistry of the phospho-rites. Chemical Geology 47, 191–220.

McKirdy, D.M., Burgess, J.M., Lemon, N.M., Yu, X.K., Cooper, A.M., Gostin, V.A., Jenkins, R.J.F., Both, R.A., 2001. A chemostratigraphic overview of the late Cryogenian interglacial sequence in the Adelaide fold-Thrust Belt, South Australia. Precambrian Research 106, 149–186.

McLennan, S.M., 1989. Rare earth elements in sedimentary rocks: influence ofprovenance and sedimentary processes. In: Lipin, B.R., McKay, G.A. (Eds.), Geo-chemistry and Mineralogy of Rare Earth Elements. Min. Soc. Am. Rev. Mineral vol. 21, pp. 169–200.

Melezhik, V.A., Fallick, A.E., 2003. $\delta^{13}C$ and $\delta^{18}O$ variations in primary and secondary carbonate phases: several contrasting examples from Paleoproterozoic 13C-rich metamorphosed dolostones. Chemical Geology 201, 213–228.

Melezhik, V.A., Gorokhov, I.M., Kuznetsov, A.B., Fallick, A.E., 2001. Chemostratigraphy of Neoproterozoic carbonates: implications for "blind dating". Terra Nova 13, 1–11.

Morad, S., Felitsyn, S., 2001. Identification of primary Ce-anomaly signatures in fossilbiogenic apatite: implication for the Cambrian oceanic anoxia and phosphogenesis. Sedimentary Geology 143, 259–264.

Mountjoy, E.W., Amthor, J.E., 1994. Has burial dolomitization come of age? Some answers from the Western Canada Sedimentary Basin. Special Publication of International Association of Sedimentologists 21, 203–229.

Narbonne, G.M., Kaufman, A.J., Knoll, A.H., 1994. Integrated chemostratigraphy and biostratigraphy of the Windermere Supergroup, northwestern Canada; implications for Neoproterozoic correlations and the early evolution of animals; with Suppl. Data 9434. Geological Society of America Bulletin 106, 1281–1292.

Notholt, A.J.G., Sheldon, R.P., Davidson, D.F., 1989. Phosphate Deposits of the World. Phosphate Rock Resources vol. 2. Cambridge Univ. Press, Cambridge, p. 566.

Nothdurft, L.D., Webb, G.E., Kamber, B.S., 2004. Rare earth element geochemistry of Late Devonian reefal carbonates, Canning Basin, Western Australia: confirmation of a seawater REE proxy in ancient limestones. Geochimica et Cosmochimica Acta 68, 263–283.

Nozaki, Y., Zhang, J., Amakawa, H., 1997. The fractionation between Y and Ho in the marine environment. Earth and Planetary Science Letters 148, 329–340.

Pankhurst, R.J., Ramos, A., Linares, E., 2003. Antiquity of the Río de la Plata craton in Tandilia, southern Buenos Aires province, Argentina. Journal of South American Earth Sciences 16, 5–13.

Poiré, D.G., 1987. Mineralogía y sedimentología de la Formación Sierras Bayas en el Núcleo Septentrional de las sierras homónimas, partido de Olavarría, provincia de Buenos Aires. Unpublisehd PhD Tesis 494. Facultad de Ciencias Naturales y Museo, Universidad Nacional de La Plata (271 pp).

Poiré, D.G., 1989. Stromatolites of the sierras Bayas Group, upper Proterozoic of Olavarría, sierras Septentrionales, Argentina. Stromatolite Newsletter 11, 58–61.

Poiré, D.G., 1993. Estratigrafía del Precámbrico sedimentario de Olavaría, Sierras Bayas, Provincia de Buenos Aires, Argentina. XII Congreso Geológico Argentino y II Congreso de Exploración de Hidrocarburos Actas II, pp. 1–11.

Poiré, D.G., Spalletti, L.A., 2005. La cubierta sedimentaria precámbrica/paleozoica inferior del Sistema de Tandilia. In: De Barrio, R.E., Etcheverry, R.O., Caballé, M.F., Llambías, E.J. (Eds.), Geología y Recursos Minerales de la provincia de Buenos Aires. Relatorio del XVI Congreso Geológico Argentino, pp. 51–68 (La Plata).

Poiré, D.G., Gaucher, C., Germs, G., 2007. La superficie "Barker" y su importancia regional, Neoproterozoico del Cratón del Río de La Plata. VI Jornadas Geológicas y Geofísicas Bonaerenses, Actas: 36 (Mar del Plata, Argentina).

Rapalini, A.E., Trindade, R.I., Poiré, D.G., 2013. The la Tinta pole revisited: paleomagnetism of the Neoproterozoic sierras Bayas Group (Argentina) and its implications for Gondwana and Rodinia. Precambrian Research 224, 51–70.

Rapela, C.W., Pankhurst, R.J., Casquet, C., Fanning, C.M., Baldo, E.G., González-Casado, J.M., Galindo, C., Dahlquist, J., 2007. The Río de la Plata Craton and the assembly of SW Gondwana. Earth Science Reviews 83, 49–82.

Rapela, C.W., Fanning, C.M., Casquet, C., Pankhurst, R.J., Spalletti, L., Poiré, D., Baldo, E.G., 2011. The Rio de la Plata craton and the adjoining Pan-African/brasiliano terranes: their origins and incorporation into south-west Gondwana. Gondwana Research 20, 673–690.

Riedgwell, A., Kennedy, M.J., Caldeira, K., 2003. Carbonate deposition, climate stability, and Neoproterozoic ice ages. Science 302, 859–862.

Rooney, A.D., Strauss, J.V., Brandon, A.D., Macdonald, F.A., 2005. A Cryogenian chronology: Two long-lasting synchronous Neoproterozoic glaciations. PALAIOS 20 (4), 348–362.

Semikhatov, M.A., 1975. Experiences in Stromatolite studies in the USSR. In: Walter, M.R. (Ed.), Stromatolites. Elsevier, Amsterdam, pp. 337–357.

Semikhatov, M.A., 1991. General problems of Proterozoic stratigraphy in the URSS. Soviet Scientific Reviews, Geology Section 1, 1–192.
Serebryakov, S.N., 1976. 4 Biotic and Abiotic Factors Controlling the Morphology of Riphean Stromatolites. Developments in Sedimentology 20, 321–336.
Shields, G., Stille, P., 2001. Diagenetic constraints on the use of cerium anomalies as palaeoseawater redox proxies: an isotopic and REE study of Cambrian phosphorites. Chemical Geology 175, 29–48.
Shields, G., Webb, G., 2004. Has the REE Composition of Seawater Changed Over Geological Time? 204, 103–107.
Shields, G.A., Deynoux, M., Culver, S.J., Brasier, M.D., Affaton, P., Vandamme, D., 2007. Neoproterozoic glaciomarine and cap dolostone facies of the southwestern Taoudéni Basin (Walidiala Valley, Senegal/Guinea, NW Africa). Comptes Rendus Geoscience 339, 186–199.
Southgate, P.N., 1989. Relationships between cyclicity and stromatolite form in the Late Proterozoic Bitter Springs Formation, Australia. Sedimentology 36 (2), 323–339.
Srinivasan, K., Walter, K.R., Goldberg, S.A., 1994. Determining fluid sourse and posible pathways during burial dolomitization of Marville limestone (Cambrian), Southern Appalachians, USA. Sedimentology 41, 293–308.
Svensen, H., Planke, S., Malthe-Sorenssen, A., Jamtveit, B., Myklebust, R., Eidem, T.R., Rey, S.S., 2004. Release of methane from a volcanic basin as a mechanism for initial Eocene global warming. Nature 429, 542–545.
Thomas, C.W., Graham, C.M., Ellam, R.M., Fallick, A.E., 2004. 87Sr/86Sr chemostratigraphy of Neoproterozoic Dalradian limestones of Scotland and Ireland: constraints on depositional ages and time scales. Journal of the Geological Society of London 161, 229–242.
Tucker, M.E., 1983. Sedimentation of organic-rich limestone in the late Precambrian of southern Norway. Precambrian Research 22, 293–315.
Tucker, M.E., Wright, V.P., 1990. Carbonate Sedimentology. Blackwell Scientific Publications, London (482 pp.).
Vahrenkamp, V.C., Swart, P., 1994. Late Cenozoic dolomites of the Bahamas: metastable analogues for the genesis of ancient platform dolomites. In: Purser, B., Tucker, M., Zenger, D. (Eds.), Dolomites — A Volume in Honor of Dolomieu. Special Publication of International Association of Sedimentologists vol. 21, pp. 133–153.
Veizer, J., 1983. Chemical diagenesis of carbonates: theory and application of trace element technique. In: Arthur, M.A., Anderson, T.F., Kaplan, I.R., Veizer, J., Land, L.S. (Eds.), Stable Isotopes in Sedimentary Geology. S.E.P.M. Short Course 10 (pp. (3–1), 3–100).
Waggoner, B., 2003. The Ediacaran biotas in space and time. Integrative and Comparative Biology 43, 104–113.
Wallace, M.W., Hood, A.V.S., Woon, E.M.S., Giddings, J.A., Fromhold, T.A., 2015. The Cryogenian Balcanoona reef complexes of the northern flinders ranges: implications for Neoproterozoic ocean chemistry. Palaeogeography, Palaeoclimatology, Palaeoecology 417:320–336. http://dx.doi.org/10.1016/j.palaeo.2014.09.028.
Walter, M.R., Veevers, J.J., Calver, C.R., Gorjan, P., Hill, A.C., 2000. Dating the 840–544 Ma Neoproterozoic interval by isotopes of strontium, carbon, and sulfur in seawater, and some interpretative models. Precambrian Research 100, 371–433.
Wang, Q., Lina, Z., Chena, D., 2014. Geochemical constraints on the origin of Doushantuo cap carbonates in the Yangtze Gorges area, South China. Sedimentary Geology 304 (56), 63–73.
Wanless, H.R., Tedesco, L.P., 1993. Depositional and early diagenetic controls on texture and fabric of carbonate mudbanks, South Florida. Carbonate microfabrics. Springer, New York, pp. 41–63.
Webb, G.E., Kamber, B.S., 2000. Rare earth elements in Holocene reefal microbialites: a new shallow seawater proxy. Geochimica et Cosmochimica Acta 64 (9), 1557–1565.
Wickham, S.M., Peters, M.T., 1993. Oxygen and carbon isotope profiles in metasediments from Lizzies Basin, East Humboldt Range, Nevada: constraints on mid-crustal metamorphic and magmatic volatile fluxes. Contributions to Mineralogy and Petrology 112, 46–65.
Wright, D.T., 1997. An organogenic origin for widespread dolomite in the Cambrian Eilean Dubh Formation, Northwestern Scotlan. Journal of Sedimentary Research 67, 54–64.
Wright, V.P., Burchette, T.P., 1998. Carbonate ramps: an introduction. 149. Geological Society, Special Publications, London, pp. 1–5.
Wright, J., Schrader, H., Holser, W.T., 1987. Paleoredox variations in ancient oceans recorded by rare earth elements in fossil apatite. Geochimica et Cosmochimica Acta 51, 613–644.
Zempolich, W.G., Baker, P.A., 1993. Experimental and natural mimetic dolomitization of aragonite ooids. Journal of Sedimentary Petrology 63, 596–606.
Zempolich, W.G., Wilkinson, B.H., Lohmann, K.C., 1988. Diagenesis of Late Proterozoic carbonates: the Beck Spring Dolomite of Eastern California. Journal of Sedimentary Petrology 58, 656–672.
Zimmermann, U., Poiré, D.G., Gómez-Peral, L.E., 2011. Neoproterozoic to lower Palaezoic successions of Tandilia system in Argentina: implication for the palaeotectonic framework of southwest Gondwana. International Journal of Earth Sciences 100, 489–510.